Nanoscale Systems MMTA • ISSN: 2299-3290
Survey Article • DOI: 10.2478/nsmmt-2012-0008 • NanoMMTA • Vol. 1 • 2012 • 112-142

VERSITA

# Mesoscopic description of boundary effects in nanoscale heat transport

F. X. Àlvarez[1*], V. A. Cimmelli[2†], D. Jou[1,3‡], A. Sellitto[2§]

1 *Departament de Física, Universitat Autònoma de Barcelona, 08193 Bellaterra, Catalonia, Spain*

2 *Department of Mathematics, Computer Science and Economics, University of Basilicata, Campus Macchia Romana, 85100 Potenza, Italy*

3 *Institut d'Estudis Catalans, Carme 47, Barcelona 08001, Catalonia, Spain*

**Abstract**

We review some of the most important phenomena due to the phonon-wall collisions in nonlocal heat transport in nanosystems, and show how they may be described through certain slip boundary conditions in phonon hydrodynamics. Heat conduction in nanowires of different cross sections and in thin layers is analyzed, and the dependence of the thermal conductivity on the geometry, as well as on the roughness is pointed out. We also analyze the effects of the roughness of the surface of the pores on the thermal conductivity of porous silicon. Thermoelectric effects are considered as well.

*In memory of Professor Carlo Cercignani*

**Keywords**

Phonon hydrodynamics • Nanosystems • Phonon-wall collisions • Effective thermal conductivity • Nonlocal heat transport

PACS: 44.10.+i,66.70.-f,05.70.Ln

MSC: 74A20, 80A17, 80A20



Received 11 October 2012
Revised 5 December 2012
Accepted in revised form 6 December 2012

## 1. Bulk and wall heat flux in nanosystems

Nowadays, the macroscopic derivation of generalized transport equations including memory and nonlocal effects has been fostered by the increasing interest in micro/nanoelectronics [23, 35, 63, 72, 81, 117, 126]. The most usual approach to these problems is a microscopic one, based on the Boltzmann equation, but here we will focus our interest on a mesoscopic approach. Indeed, there is a current interest for mesoscopic modelizations based on generalized heat transport equations simpler than the much more complex and detailed microscopic approach. Three such approaches are the so-called phonon hydrodynamics [28–30], the so-called thermomass theory [18, 46, 47], and the dual-lag model [117, 118]. These models consider the heat carriers as a fluid whose hydrodynamic-like equations describe the heat transport. Here we will address mainly the phonon-hydrodynamic model because it has paid more attention to boundary conditions, since the corresponding heat-transfer equation contains a nonlocal term of higher order than in the thermomass theory. The thermomass heat transfer equation will be briefly commented at the end of the paper.

In the linear regime the phonon hydrodynamics, wherein the phonons represent the main heat carriers, is based on the Guyer-Krumhansl transport equation [1, 26, 27, 49, 50, 63, 118] for the heat flux $\mathbf{q}$, i.e.,

$$\tau\dot{\mathbf{q}} + \mathbf{q} = -\kappa_0 \nabla T + \ell^2 \left(\nabla^2 \mathbf{q} + 2\nabla\nabla\cdot\mathbf{q}\right), \tag{1}$$

where $\tau$ is the relaxation time due to the resistive (quasi-momentum not conserved) scattering of phonons in the bulk, $T$ is the temperature, and $\ell$ is the mean-free path (mfp). Moreover, in Eq. (1) $\kappa_0$ represents the Ziman limit [129] for

* *E-mail: xavier.alvarez@uab.es*
† *E-mail: vito.cimmelli@unibas.it*
‡ *E-mail: david.jou@uab.es*
§ *E-mail: ant.sellitto@gmail.com*

the bulk thermal conductivity, namely, $\kappa_0 = \varrho c_v \tau \bar{c}^2/3$, where $\varrho$ is the mass density, $c_v$ is the specific heat per unit mass at constant volume, and $\bar{c}$ is the average speed of phonons. Although we refer to Eq. (1) as the Guyer-Krumhansl equation, it is worth noticing that it has in fact important differences with respect to the original proposal of Guyer and Krumhansl [1, 49, 50], the main being the way as boundary conditions are included in the model. Originally, those authors considered a boundary relaxation-time $\tau_b$ that they added to the usual relaxation time due to resistive mechanisms by the use of Matthiessen rule as $\tau^{-1} = \tau_u^{-1} + \tau_i^{-1} + \tau_d^{-1} + \tau_b^{-1}$, with $\tau_u$ being the relaxation time of umklapp-phonon collisions, $\tau_i$ being the relaxation time of phonon-impurity collisions, and $\tau_d$ being the relaxation time of phonon-defect collisions. Once the combined resistive-boundary collision time was obtained, the thermal conductivity $\kappa$ (depending on the size of the system through the $\tau_b$-dependence of $\tau$) was obtained and used in the first term of the right-hand side of Eq. (1), instead of $\kappa_0$. Moreover, the mfp $\ell$ was calculated as $\ell^2 = \bar{c}^2 \tau_N \tau/5$, where $\tau_N$ is the relaxation time of normal (momentum conserving) interactions between phonons. In what follows, we do not include the boundary collision time $\tau_b$ in the differential equation (1), but in suitable boundary constitutive equations [2, 73, 101, 102].

Following this approach, the resistive relaxation time may be evaluated as $\tau^{-1} = \tau_u^{-1} + \tau_i^{-1} + \tau_d^{-1}$, the mfp appearing in Eq. (1) is calculated by the usual resistive value $\ell = \bar{c}\tau$, and therein the bulk thermal conductivity $\kappa_0$ is used instead of $\kappa$. Therefore, when in the next we refer to Eq. (1) as the Guyer-Krumhansl equation, it will be understood that we are referring to its mathematical form, rather than to the interpretation of the coefficients appearing in it. In this review paper, we focus our attention on the modelization of the constitutive equations for a slip heat flux along the walls necessary to complement Eq. (1) and its many consequences.

Equation (1) generalizes the classical Fourier equation

$$\mathbf{q} = -\kappa_0 \nabla T, \tag{2}$$

by including both relaxation effects (characterized by the relaxation time $\tau$), and nonlocal effects (characterized by the mfp $\ell$), in such a way that when these effects are negligible, Eq. (1) reduces to Eq. (2). Indeed, whenever only nonlocal effects are negligible in heat propagation, Eq. (1) turns out the Maxwell-Cattaneo-Vernotte equation [19, 20]

$$\tau \dot{\mathbf{q}} + \mathbf{q} = -\kappa_0 \nabla T, \tag{3}$$

which accounts for heat conduction with finite speed of thermal disturbances [25, 112].

In the microscopic approach Eq. (1) has been derived by solving the linearized Boltzmann equation for phonons [1, 23, 49, 50]. As a consequence, it is not suitable to account for nonlinear effects, which instead are usual at the micro/nanoscale, since even small differences of temperature, over a reduced length-scale may produce strong gradients. However, extensions of Eq. (1) to the nonlinear regime may be obtained in the framework of Extended Irreversible Thermodynamics [27, 29, 30, 71], a theory which upgrades the dissipative fluxes to the rank of independent thermodynamic variables [62, 63, 72, 73], while nonlinear generalizations of Eq. (3) have been obtained in the framework of the thermomass theory [18, 46, 47], which also pays a special attention to nonlinear terms in the heat transport equation.

The analysis of heat conduction in rigid bodies (as one may consider nanosystems) requires to complement Eq. (1) by the local balance of the energy which, in the absence of external sources reads

$$\dot{u} + \nabla \cdot \mathbf{q} = 0, \tag{4}$$

with $u$ being the internal energy per unit volume. In particular, when Eq. (4) is taken into account in the last term of Eq. (1), in the steady state the latter reduces to the following nonlocal constitutive equation for the heat flux:

$$\mathbf{q} = -\kappa_0 \nabla T + \ell^2 \nabla^2 \mathbf{q}. \tag{5}$$

In nanosystems one may have on many occasions that the characteristic size $d$ of the systems is considerably smaller than $\ell$, and therefore, in Eq. (5), one can often neglect the heat flux $\mathbf{q}$ with respect to $\ell^2 \nabla^2 \mathbf{q}$. In fact, since in nanosystems $\ell^2 \nabla^2 \mathbf{q} \approx \mathrm{Kn}^2 \mathbf{q} \gg \mathbf{q}$, with the Knudsen number $\mathrm{Kn} = \ell/d$ generally reaching values of the order of 1 (or relatively higher than 1), the nonlocal term in Eq. (5) may be more important than the heat flux itself [2, 4, 101, 102], and that equation reduces to

$$\nabla^2 \mathbf{q} = \frac{\kappa_0}{\ell^2} \nabla T. \tag{6}$$

Equation (6) is analogous to the Navier-Stokes equation for steady states and for those situations in which the nonlinear convective term is null (or may be negligible), i.e.,

$$\nabla^2 \mathbf{v} = \frac{1}{\eta} \nabla p, \tag{7}$$

$\eta$ being the shear viscosity of the fluid, $\mathbf{v}$ is the velocity of the fluid, and $p$ is the pressure. The analytical resemblance between Eqs. (6) and (7) motivates the definition of "hydrodynamic regime" for those situations in which the heat flux obeys Eq. (6), and allows one to identify the "viscosity" of phonons in terms of the thermal conductivity and the mfp.

In what follows we limit ourselves to consider only nanosystems in the linear regime, so that either Eq. (1), or one of its stationary versions (5) and (6), hold. Indeed, Eqs. (1) and (6) are second-order (in space) partial differential equations whose solution can be achieved only if suitable boundary conditions are given. We will assume for simplicity that the heat loss across the lateral walls is negligible. Notwithstanding, due to the several phonon-wall collisions, a slip-flow contribution along the wall $\mathbf{q}_w$ additional to the bulk heat flux should be expected. This wall heat flux, in general, is restricted only to a thin region near the walls (the so-called Knudsen layer), whose thickness is of the order of the phonon mfp. Far from the wall it may be neglected. However, in nanosystems of dimension comparable to (or smaller than) $\ell$, $\mathbf{q}_w$ will extend in the whole system and it may be assumed as a constant contribution.

To evaluate it, helpful suggestions can be achieved from microfluidics [15]. This is a new interdisciplinary field of research that is concerned with the handling and transport of small amounts (nano/picoliters) of liquid. Its main task is the reproduction on a chip of millimetric size of all operations (synthesis, separation, analysis ...) that currently require the use of various laboratories. Regardless of achieving this ambitious goal, microfluidic chips are already used in many laboratories for the considerable advantages which are all derived from low-volume fluid treated [84]. For example, these devices provide portability, a high control of flows, a reduction in the time to synthesize and analyze a product. A very promising field in the microfluidics perspectives is the "droplet logic", a new area of research in which a drop of liquid moving in a microchannel represents one bit. This allows to perform logical operations through the transport of material. In Tab. 1 the main analogies between integrated circuits and microfluidic chips are pointed out [88].

***Table 1.*** Analogies between integrated circuits and microfluidic chips.

| | **Integrated circuit** | **Microfluidic chip** |
|---|---|---|
| Transported quantity | Energy | Mass |
| Material | Semiconductors (inorganic) | Polymers (organic) |
| Channel size | nm | $\mu$m |
| Transport regime | Phonon hydrodynamics | Laminar fluid-dynamics |

In microfluidics, the behavior of the fluid in the center of the tubes is governed by the usual Navier-Stokes equations. Along the surface it is not always assumed the usual non-slip condition for the velocity (i.e., vanishing velocity along the wall) but a slip flow is assumed in principle. The two mostly-used types of boundary conditions are:

$$\mathbf{v}_w = c l' \frac{\partial \mathbf{v}_b}{\partial \xi}, \qquad \text{First-order slip condition} \tag{8a}$$

$$\mathbf{v}_w = c l' \frac{\partial \mathbf{v}_b}{\partial \xi} - a l'^2 \frac{\partial^2 \mathbf{v}_b}{\partial \xi^2}. \qquad \text{Second-order slip condition} \tag{8b}$$

In the equations above $\mathbf{v}_w$ and $\mathbf{v}_b$ represent, respectively, the velocity of the fluid on the wall of the microchannel containing the fluid and in the bulk, $l'$ is the mfp of the particles, and $\xi$ means the outward normal direction to the boundary. Moreover, $c$ and $a$ are positive constants, related to the properties of the walls [22, 44, 113]. Cercignani was the first to propose a second-order slip condition of the type (8b) in rarefied gas dynamics, and his model is in good agreement with solutions of the linearized Boltzmann equation for a hard-sphere gas in a wide range of rarefaction [21, 51]. In the hydrodynamic context, the first-order slip model (8a) is also known as Maxwell slip model [16, 68]. Whenever the second-order slip model (8b) is used, instead, it is speaking about the so-called second-order slip model [57] when $a = 1/2$, and it is speaking about the so-called 1.5-model [89] when $a = 2/9$.

Due to the analogies mentioned above, the following first- and second-order constitutive equations for $\mathbf{q}_w$ have been recently proposed by Jou and co-workers [2, 4, 66, 101–104, 108] for nanosystems:

$$\mathbf{q}_w = C\ell \frac{\partial \mathbf{q}_b}{\partial \xi}, \tag{9a}$$

$$\mathbf{q}_w = C\ell \frac{\partial \mathbf{q}_b}{\partial \xi} - \alpha \ell^2 \frac{\partial^2 \mathbf{q}_b}{\partial \xi^2}, \tag{9b}$$

where $\mathbf{q}_w$ and $\mathbf{q}_b$ represent, respectively, the wall contribution to the local heat flux and the bulk one. Moreover $C$ and $\alpha$ are positive constants, related to the properties of the walls. In Refs. [2, 4, 66, 101–104, 108] these conditions are used in non-standard way, assuming that the overall heat flux is given by $\mathbf{q} = \mathbf{q}_b + \mathbf{q}_w$. Thus, in steady-state situations the local heat flux $\mathbf{q}$ can be calculated as follows: first, one can solve either Eq. (5) (if Kn is less than, or comparable to, 1) or Eq. (6) (if Kn is larger than 1) with vanishing heat flux on the boundary. Then, the additional flux $\mathbf{q}_w$ (still given by one of Eqs. (9)) is added to $\mathbf{q}_b$. It is usually admitted that $\mathbf{q}$ takes the value $\mathbf{q}_b$ in the bulk and $\mathbf{q}_w$ at the wall: although boundary conditions strongly determine the behavior of a system, one could nevertheless expect that the thermal conductivity is depending on $\mathbf{q}_b$ in the bulk, and on $\mathbf{q}_w$ on the wall. Indeed, from the physical point of view, the boundary is never a true surface, but rather a thin layer, whose dimension is of the order of magnitude of the mfp of the heat carriers (that is, the Knudsen layer). On the other hand, due to the small dimensions of the systems at hand, the Knudsen layer pervades the whole system, so that the heat flux on the boundary, i.e., in the Knudsen layer, is superposed to the heat flux in the bulk. This fact suggests to assume $\mathbf{q} = \mathbf{q}_b + \mathbf{q}_w$ as the overall heat flux and suppose that the thermal conductivity depends on it.

In an extension of Ref. [65], Lebon *et al.* [74] have carried out a separate thermodynamic analysis of the constitutive equations for bulk and wall heat flux. Though in steady states the effective thermal conductivity is a macroscopic quantity in which both bulk effects and boundary effects are superposed, both contributions could be in principle differentiated if one combines steady-state results with frequency-dependent thermal conductivity [103], heat wave analyses [66], and heat fluctuations [65, 82], which provide independent information. Up to now, however, we are not aware of experimental measurements.

Although heuristic, the method allows to take into account the phonon-wall interactions in nanosystems [64] still remaining in a macroscopic framework. Moreover, it is conceptually appealing since it uses well-known results of rarefied gas dynamics, but applied to a phonon gas [23, 64].

The coefficient $C$ describes the specular and diffusive collisions of the phonons with the walls, whereas $\alpha$ accounts for phonon backscattering. Both coefficients are temperature dependent and are related to the properties of the walls [101, 102], which may be smooth or rough [40]. In particular, as it has been pointed out in Ref. [101], the second-order constitutive equation (9b) allows to predict a minimum radius for the transversal section of a nanowire (see Eq. (17) therein), in such a way that if the characteristic size of the system becomes smaller than that value, the system at hand stops to be a conductor and becomes an insulator. This recalls the idea of the metal-insulator Anderson transition [33, 42].

More general situations can be treated at the price of more mathematical complexity. For instance, in nanowires undergoing high-frequency perturbations, it is necessary to assume a relaxation of the heat flux on the boundary too (analogous to the relaxation term appearing in the Maxwell-Cattaneo (3), but referred to the slip heat flux), through a dynamical constitutive equation of the type [66]

$$\tau_w \dot{\mathbf{q}}_w + \mathbf{q}_w = C\ell \frac{\partial \mathbf{q}_b}{\partial \xi} - \alpha \ell^2 \frac{\partial^2 \mathbf{q}_b}{\partial \xi^2}. \tag{10}$$

In Eq. (10) $\tau_w$ represents a suitable relaxation time accounting for the frequency of phonon-wall collisions. Since these interactions may produce specular, diffusive and backward reflections of the phonons, the Matthiessen's rule yields $\tau_w^{-1} = \tau_{spec}^{-1} + \tau_{diff}^{-1} + \tau_{back}^{-1}$, where $\tau_{spec}$, $\tau_{diff}$ and $\tau_{back}$ refer to the characteristic time of specular collisions, diffuse collisions and backscattering, respectively.

It is possible to obtain a qualitative estimation of $\tau_w$ by evaluating the total frequency of collisions between phonons and walls. Since a wall, in principle, has both smooth regions of width $D$ and rough regions of peaks $\Delta$ (see Fig. 1 for a qualitative sketch of the wall features), in a tentative way it is possible to write

$$\frac{1}{\tau_w} = \frac{\bar{c}}{d}\left(\frac{D}{D+\Delta}\right) + \frac{\bar{c}}{d-\Delta}\left(\frac{\Delta}{D+\Delta}\right). \tag{11}$$

In Eq. (11) the ratio $D/(D+\Delta)$ indicates the probability of finding a smooth region, and $\Delta/(D+\Delta)$ the probability of finding a peak (we are assuming for the sake of simplicity that the width of the peaks is proportional to their height). In the case of smooth walls (i.e., when $\Delta/D \to 0$), one has $\tau_w = R/\bar{c}$. In the limit case of very rough walls (i.e., when $\Delta \to R$), $\tau_w = 0$: the phonons cannot advance in the nanowire because there is no free space to go ahead.

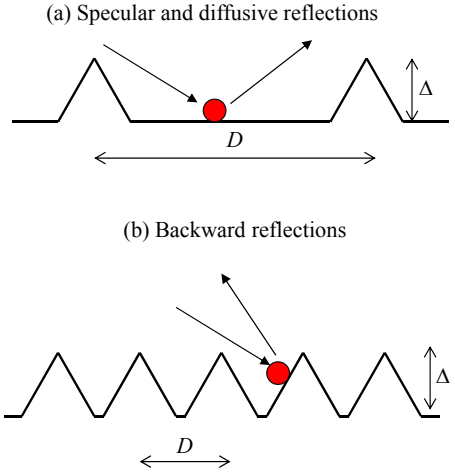


***Fig 1.*** Different degree of roughness of a wall, described by the parameters $\Delta$ (height of the roughness peaks) and $D$ (separation of neighboring roughness peaks). When the ratio $\Delta/D \to 0$ (or in the limit case when $\Delta = 0\,\mathrm{nm}$), only specular and diffusive scattering is expected (Fig. 1a). Otherwise, backscattering is expected (Fig. 1b). Furthermore, when $D = \Delta$ the surface has no flat regions, but it is completely rough. In figure, the red circle represents the heat carrier.

We observe that suitable boundary conditions are also important to study fluctuations of the heat flux, or other fluxes, which are expected to be important because of the small sizes involved in nanosystems. In particular, in Ref. [64] the second moment of fluctuations around equilibrium systems is studied. This is a topic which is well known for diffusive transport equations through the fluctuation-dissipation theorem but less explored for ballistic transport, with strong influence of boundary effects.

Another interesting situation is the simultaneous transfer of thermal and electric current, due to the motion along the conductor of two different types of heat carriers: phonons and electrons. In such a case it is possible the conversion of heat current into electric current through thermoelectric effects, i.e., the direct conversion of temperature differences to electric voltage and vice-versa [8, 10, 13, 36, 109, 115]. In fact, a thermoelectric device is capable to create a voltage whenever there is a different temperature on each side and, conversely, when a voltage is applied to it, a temperature difference arises. The term thermoelectric effect encompasses two different phenomena: the Peltier effect, i.e., the exchange of heat at an electrified junction of two different metals, and the Seebeck effect, namely, the conversion of temperature differences directly into electricity. The combination of both these effects could yield, in total, big amounts of available electric energy by the application of relatively small temperature differences across thin interfaces separating different materials. The thermodynamic efficiency of this type of devices may be evaluated through the dimensionless parameter $ZT$, with $T$ being the absolute temperature, and $Z$ is the so-called figure-of-merit [9, 31, 58, 60, 91, 94], defined as

$$Z = \frac{\epsilon^2 \sigma_e}{\kappa_e + \kappa_p}, \tag{12}$$

wherein $\epsilon$ is the Seebeck coefficient, $\sigma_e$ is the electrical conductivity, and $\kappa_e$ and $\kappa_p$ are the thermal conductivities due to electrons and phonons, respectively [111]. Since a larger value of $ZT$ indicates a greater thermodynamic efficiency [72], the evaluation of $ZT$ is important for comparing the potential efficiency of devices using different materials.

One of the most explored possibilities is the junction of two nanostructured crystals of different type (as for example nanowires made of InSb, InAs, GaAs and InP), in which the heat is carried by phonons and electrons. This problem can be addressed from a microscopic point of view by solving the Boltzmann equation for phonons and electrons [78, 86, 87, 121]. However, as a first and easy step in the analysis of thermoelectric effects, one should look for generalized transport equations describing heat and electric transport with thermoelectric coupling. In this light, a helpful working hypothesis

is that the heat flux $\mathbf{q}$ has two different contributions: the phonon heat flux $\mathbf{q}^{(p)}$ and the electron heat flux $\mathbf{q}^{(e)}$, such that $\mathbf{q} = \mathbf{q}^{(p)} + \mathbf{q}^{(e)}$. Thus, the following partial energy balances hold

$$\dot{u}^{(p)} + \nabla \cdot \mathbf{q}^{(p)} = 0, \tag{13a}$$
$$\dot{u}^{(e)} + \nabla \cdot \mathbf{q}^{(e)} = \mathbf{E} \cdot \mathbf{I}, \tag{13b}$$

where $u^{(p)}$ and $u^{(e)}$ are the partial internal energies per unit of volume, $\mathbf{E}$ is the electric field, and $\mathbf{I}$ is the electric-current density. For non-polarized materials, beside Eqs. (13), additional evolution equations for the fluxes $\mathbf{q}^{(p)}$, $\mathbf{q}^{(e)}$ and $\mathbf{I}$ are needed, and we take for them the following nonlocal expressions [67]

$$\tau_p \dot{\mathbf{q}}^{(p)} + \mathbf{q}^{(p)} = -\kappa_p \nabla T + \ell_p^2 \left( \nabla^2 \mathbf{q}^{(p)} + 2 \nabla \nabla \cdot \mathbf{q}^{(p)} \right), \tag{14a}$$
$$\tau_e \dot{\mathbf{q}}^{(e)} + \mathbf{q}^{(e)} = -\left( \kappa_e + \epsilon \Pi \sigma_e \right) \nabla T + \ell_e^2 \left( \nabla^2 \mathbf{q}^{(e)} + 2 \nabla \nabla \cdot \mathbf{q}^{(e)} \right) + \Pi \sigma_e \mathbf{E}, \tag{14b}$$
$$\tau_I \dot{\mathbf{I}} + \mathbf{I} = \sigma_e \left( \mathbf{E} - \epsilon \nabla T \right) + \ell_I^2 \left( \nabla^2 \mathbf{I} + 2 \nabla \nabla \cdot \mathbf{I} \right), \tag{14c}$$

where $\left(\tau_p; \ell_p\right)$, $(\tau_e; \ell_e)$ and $(\tau_I; \ell_I)$ are the relaxation time and the mfp of phonons, electrons and electric current [49, 50, 56, 67], respectively, while $\Pi$ is the Peltier coefficient. The model above, when complemented with the constitutive equations (9), allows to describe the size dependency of the figure-of-merit in cylindrical nanowires.

A further problem which deserves consideration is the pore-size dependency of the thermal conductivity in porous silicon (pSi), namely, a form of the chemical element silicon in a microstructure in which the pores have been generated by a suitable chemical process. Porous silicon was discovered in 1956 by Uhlir [120], although significant interest in this material is only recent, due to the work by Canham [17] demonstrating the room-temperature photoluminescence properties of pSi, which fostered the attention of the scientific community and firstly stimulated research on its use for optoelectronic circuits. Nowadays, the use of pSi may be found in Light Emitting Diodes (LEDs), electronics and sensors. Recently, pSi has also become of much interest in nanoscale heat transport [23, 117, 126]. The optimization of its use in practical applications requires a good knowledge about its thermal properties. Among all the thermal properties, special attention has been paid to the thermal conductivity for the use of pSi as device isolation in integrated circuits [59, 122]. In fact, the pSi thermal conductivity has been measured to be two to five orders of magnitude smaller than that of the bulk silicon, and decreases greatly for increasing porosity [11, 24, 43, 76, 110], that is, the volume fraction corresponding to the pores.

The simplest theoretical model prescribes that the thermal-conductivity of a porous medium $\kappa_t$ depends only on the porosity $\phi$ [95], as

$$\kappa_t = f(\phi)\, \kappa_0, \tag{15}$$

with $f(\phi)$ being a suitable function of the porosity, whose value is smaller than 1. Different models differ from each other in the form of this function [43, 80, 114]. Indeed, we can show that, if the models above are enriched by introducing the role of the pores (characteristic sizes, internal rearrangement and their rugosity), the theoretical values of the thermal conductivity are closer to the measured ones.

In the present paper we review the main results which can be obtained, in different situations, by applying one of the non-standard constitutive equations for $\mathbf{q}_w$ illustrated above to nanowires, nanotubes or thin layers. To this end we analyze the most essential physical parameter related to the heat conduction in nanosystems, i.e., the effective heat conductivity. For a nanosystem of length $L$ and cross section of area $A$, at the ends of which a difference of temperature $\Delta T$ is applied, and through which a total heat per unit of time $Q_{tot}$ is flowing, the effective thermal conductivity is defined as

$$\kappa_{eff} = \frac{Q_{tot}}{A} \frac{L}{\Delta T}. \tag{16}$$

In analogous way it is possible to define other effective parameters, such as the effective electrical conductivity or the effective Seebeck coefficient. The importance of such effective coefficients lays on the fact that they represent what can be measured in practice. Later, we will show that they can depend on several parameters as, for instance, the geometrical shape of the system, the frequency of the initial heat impulse, as well as the roughness of the walls. These dependencies still will be pointed out owing to the application of the constitutive equations for $\mathbf{q}_w$ introduced by Eqs. (9).

It seems important to stress that the theoretical results of the present review are not completely conclusive on this point, as they do not incorporate quantum localization effects, which may play a very relevant role when the characteristic size of the system becomes comparable to (or less than) the predominant phonon wavelength, which is inversely proportional to the absolute temperature. Since at temperature of 10 K the predominant phonon wavelength is of the order of a few nanometers, it turns out that quantum localization effects are expected to be very important only for very low temperatures or very thin nanowires, which will not be considered here. Thus, we explicitly note that the mesoscopic approach used here to estimate the size effects does not aim to replace either the quantum theory, or the fundamental physics at nanoscale, which are much detailed approaches. From the practical point of view, this approach must be understood only as an easy and fast tool, providing a relatively simple first analysis of some of the most promising situations, which afterward should be studied in deeper detail.

In Sec. 2 we consider nanowires and thin layers of different cross sections, and show how the geometry of the cross section, as well as its dimensions, may influence the value of the effective thermal conductivity.

In Sec. 3 we analyze more refined models of walls, pointing out the dependence of the effective thermal conductivity on the roughness, which may be incorporated in the coefficients $C$ and $\alpha$.

In Sec. 4 we focus on non-steady situations, generated by a time-dependent boundary heat impulse. By combining the phonon-hydrodynamic approach with the dynamical constitutive equation (10) we show how, in such a case, the effective thermal conductivity depends on the frequency of the boundary heat impulse.

In Sec. 5 we study the thermoelectric effects by applying the system (14) together with the first-order constitutive equation (9a), in order to point out the dependence of the figure-of merit of cylindrical nanowires on the radius.

In Sec. 6 we use the phonon-hydrodynamic approach to estimate the pores dependence of the effective thermal conductivity in porous silicon. We show that theoretical predictions including the role of the pores better fit with experimental values, in comparison with theoretical predictions which do not account for the role of the pores.

In Sec. 7 we review some open problems, both theoretical and applied, which deserve consideration and that should be analyzed in future research. Moreover, in this section we point out the main feature of another mesoscopic approach in heat transport at nanoscale, that is, the thermomass theory [18, 34, 46, 47, 118, 119, 124] which also deserves a closer attention.

## 2. Geometrical dependence of the effective thermal conductivity

One of the most well-known observations in small systems is that the effective thermal conductivity depends not only on the material, but also on the geometry of the system, both in the size as in the shape. To describe the experimental results on such geometrical dependence one can use the kinetic theory of phonons in small systems, or the molecular dynamical simulations, or the mesoscopic transport theories. Such a dependency does not contradict the general principles of continuum physics. Indeed, since in classical mechanics the size and the shape of the bodies are frame-invariant, the so-called principle of frame-indifference, widely used in continuum mechanics [72], which states that the response of a system should be invariant under motions of the observer, namely, under translations and rotations of the observer, is respected in such a case.

First, let us consider the thermal conductivity of thin layers of rectangular cross section, by analyzing the propagation of longitudinal heat flux in steady-state situations, and let us suppose that the longitudinal length $L$ is much larger than the other characteristic sizes (see Fig. 2 for a qualitative sketch).

As a first approximation one may suppose that the width $w$ of the cross section is much larger than its thickness $h$. In this case, the bulk heat-flow profile following from Eq. (5) reads [2]

$$q_{\mathrm{b}}(y) = \kappa_0 \left(1 - \frac{e^{\frac{y}{\ell}} + e^{-\frac{y}{\ell}}}{e^{\frac{h}{2\ell}} + e^{-\frac{h}{2\ell}}}\right) \frac{\Delta T}{L}, \tag{17}$$

where $y$ is the axis perpendicular to the parallel plates and spans the range from $-h/2$ to $h/2$. According to Eq. (9a), the wall contribution is given by

$$q_{\mathrm{w}}(y) = \kappa_0 C \tanh\left(\frac{h}{2l}\right) \left(\frac{e^{\frac{y}{\ell}} + e^{-\frac{y}{\ell}}}{e^{\frac{h}{2\ell}} + e^{-\frac{h}{2\ell}}}\right) \frac{\Delta T}{L}. \tag{18}$$

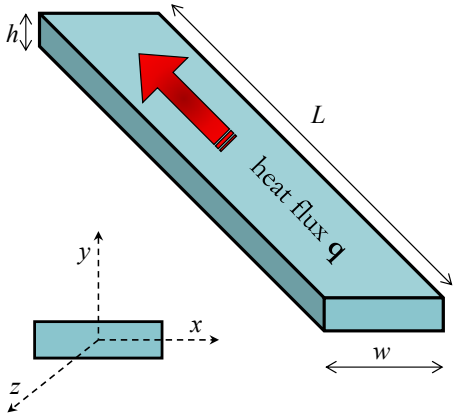


***Fig 2.*** Thin layer with a rectangular cross section. The system of coordinates in each transversal section is such that $x \in [-w/2; w/2]$, and $y \in [-h/2; h/2]$. The length $L$ of the layer is much larger than $h$ and $w$. The heat is flowing along the longitudinal axis $z$.

Consequently, from Eq. (16) in Ref. [104] the following effective thermal conductivity has been obtained

$$\kappa_{\text{eff}}(\text{Kn}) = \kappa_0 \left\{1 - 2\,\text{Kn}\tanh\left(\frac{1}{2\,\text{Kn}}\right)\left[1 - C\tanh\left(\frac{1}{2\,\text{Kn}}\right)\right]\right\}, \tag{19}$$

with $\text{Kn} = \ell/h$ in this case. When Kn gets high values, Eq. (19) reduces to

$$\kappa_{\text{eff}}(\text{Kn}) = \frac{\kappa_0}{12\,\text{Kn}^2}(1 + 6C\,\text{Kn}), \tag{20}$$

which predicts a linear decrease of the effective thermal conductivity in terms of $h$ (i.e., in terms of $\text{Kn}^{-1}$) whenever $\text{Kn} \to \infty$, in agreement with experimental measurements [6, 12, 77, 79, 116]. Without the inclusion of the boundary heat flux expressed by Eq. (18) (i.e., $C = 0$ in Eq. (20)), the effective thermal conductivity would be predicted to decrease quadratically with respect to the reciprocal of the Knudsen number, against the experimental evidence. This shows the relevance of complementing Eq. (1) with Eqs. (9) for the boundary conditions on the slip heat flux. As shown in Ref. [2] the same behavior as in Eq. (20) for the effective thermal conductivity could be obtained when Eq. (6) is considered, instead of Eq. (5).

Of course, in practical applications, the rectangular cross section of a thin layer has a finite width. If we remove the hypothesis $w \to \infty$ and suppose it has a finite value (comparable to the value of $h$), the following expression for the effective heat conductivity can be achieved

$$\kappa_{\text{eff}}(\text{Kn}) = \frac{\kappa_0}{12\,\text{Kn}^2}\left[1 - \frac{192}{\pi^5}\gamma\sum_{t,\text{odd}}^{\infty}\frac{1}{t^5}\tanh\left(\frac{t\pi}{2\gamma}\right)\right] + \frac{\kappa_0}{2\,\text{Kn}}\left[1 - \frac{8}{\pi^3}\gamma\sum_{t,\text{odd}}^{\infty}\frac{1}{t^3}\tanh\left(\frac{t\pi}{2\gamma}\right)\right]C, \tag{21}$$

where $\gamma$ here means the ratio $h/w$. Up to the first-order approximation in $\gamma$, Eq. (21) reduces to

$$\kappa_{\text{eff}}(\text{Kn}) = \frac{\kappa_0}{12\,\text{Kn}^2}\left[1 - 0.630\gamma + 6C\,\text{Kn}\,(1 - 0.271\gamma)\right]. \tag{22}$$

Note the very close behavior of $\kappa_{\text{eff}}$ predicted by Eq. (22) with that of Eq. (20), the sole difference between these behaviors lying on the presence of the shape factor $\gamma$. Increasing values of $\gamma$ yield a reduction in the effective thermal

conductivity, for a given value of $h$ (or of Kn), because this means a reduction of $w$ and, therefore, an increase of the phonon-wall collisions with the lateral walls.

An analogous analysis may be carried out in the case of circular and elliptical smooth-walled nanowires. These structures, made of either metallic (e.g., Ni, Pt, Au), or semiconducting (e.g., Si, InP, GaN, etc.), or insulating (e.g., $SiO_2$, $TiO_2$) materials, have a thickness or diameter constrained to tens of nanometers, and an unconstrained length. Let us start our analysis by considering nanowires of elliptical cross section. Without loss of generality, we assume $2a$ as the major axis, and $2b$ as the minor one (see Fig. 3 for a qualitative sketch of the transversal section).

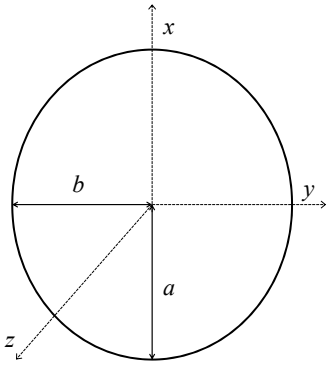


***Fig 3.*** Nanowire with an elliptical cross section. The length $L$ of the nanowire is much larger than the sizes of the cross section and the heat is flowing along the longitudinal $z$-axis. In figure the system of coordinates is also shown.

We assume that the nanowire's length $L$ is significantly larger than $a$. We still analyze steady-state situations and the longitudinal heat flow along the $z$ axis. Moreover, for the sake of simplicity, we suppose $\mathrm{Kn} \gg 1$ where, by taking as characteristic length that of the minor semi-axis, Kn is now defined as $\ell/b$. This is a natural assumption, because the predominant phonon-wall collisions will be those corresponding to the thinner dimension. In this case, the hydrodynamic results yield for the bulk heat flux [45]

$$q_{\mathrm{b}}(x;y) = \frac{\kappa_0}{2}\frac{b^2}{\ell^2}\left(\frac{1}{1+\Phi^2}\right)\left(1-\frac{x^2}{a^2}-\frac{y^2}{b^2}\right)\frac{\Delta T}{L}, \tag{23}$$

where $\Phi = b/a$. Analogously, from Eq. (9a) one may get the following wall contribution

$$q_{\mathrm{w}}(x) = \kappa_0\frac{b}{\ell}\left(\frac{C}{1+\Phi^2}\right)\left[\sqrt{\frac{x^2}{a^2}(\Phi^2-1)+1}\right]\frac{\Delta T}{L}, \tag{24}$$

in order to have [104]

$$\kappa_{\mathrm{eff}}(\mathrm{Kn}) = \frac{\kappa_0}{2\,\mathrm{Kn}}\left[\frac{1}{2\,\mathrm{Kn}}\left(\frac{1}{1+\Phi^2}\right)+CS(\phi)\right], \tag{25}$$

with $S(\Phi)$ being a numerical correction for the heat flux at the walls given by [45]

$$S(\Phi) = 1-0.6976\left[\frac{\Phi^2-1}{1.951\Phi^2+1}\right]. \tag{26}$$

In Fig. 4 we plot the behavior, arising from Eq. (25), of the effective thermal conductivity in elliptical silicon nanowires at 100 K ($\kappa_0 = 884\,\mathrm{Wm^{-1}K^{-1}}$, $\ell = 557\,\mathrm{nm}$), as a function of the ratio $\Phi = b/a$. The results in Fig. 4 show that

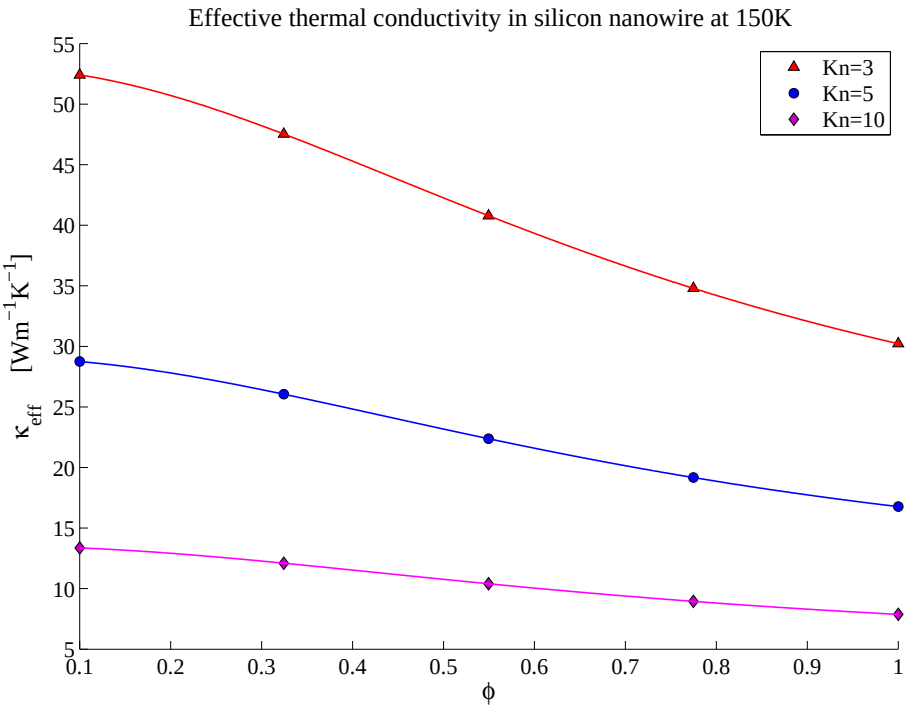


***Fig 4.*** Effective thermal conductivity in nanowires with an elliptical cross section as a function of $\Phi$ following from Eq. (25). The nanowire is made of silicon at 150 K. Three different values of the Knudsen number have been considered (that is, $\mathrm{Kn} = 3$, $\mathrm{Kn} = 5$ and $\mathrm{Kn} = 10$). Since in our approach $\mathrm{Kn} = \ell/b$, changes in $\Phi$ are only due to changes in $a$.

whenever the shape of the cross section varies, the effective thermal conductivity changes. In particular, the smaller $\Phi$ the greater $\kappa_{\mathrm{eff}}$.

Finally, let us focus our attention on a nanowire with a circular cross section of radius $R$, with $R \ll L$. A sketch of the geometry is shown in Fig. 5, where the Knudsen layer, as well as the system of coordinates, are shown.

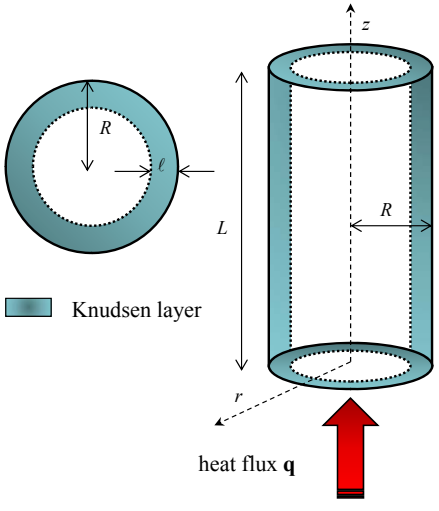


***Fig 5.*** Cylindrical nanowire with a $R$-circular cross section. The length $L$ of the nanowire is much larger than the size of the cross section. The heat (red arrow in figure) is flowing along the longitudinal axis. In figure it is also shown the Knudsen layer near the walls. In this layer, the characteristic width of which is of the order of the phonon mfp, the wall contribution to the local heat flux is more relevant than outside.

We restrict our attention to steady-state situations and suppose that heat may only flow along the longitudinal direction of the sample. The latter assumption is recovered whenever $R \ll L$. Moreover, also the end effects may be neglected so that Eq. (1) reduces to

$$q = -\kappa_0 \nabla_z T + \ell^2 \nabla^2 q, \tag{27}$$

where $\nabla_z$ is the component of $\nabla$ operator along the $z$ axis (see Fig. 5). In Eq. (27) the longitudinal heat flux $q$ may vary in the transversal section, namely, $q = q(r)$, with $r$ being the radial distance to the axis, whereas we suppose $\nabla_z T$ constant in each transversal section. By imposing $q_b(R) = 0$, the solution of Eq. (27) is [2, 104]:

$$q_b(r) = \kappa_0 \left[1 - \frac{J_0(ir/\ell)}{J_0(iR/\ell)}\right] \frac{\Delta T}{L}, \tag{28}$$

where we have written $\nabla_z T = -\Delta T/L$ along the axis of the system, and $J_0(z)$ means the zero-order cylindrical Bessel function of the indicated argument. Taking into account the first-order constitutive equation (9a), then the wall contribution is

$$q_w(r) = -\kappa_0 \left\{ C \left[\frac{iJ_1(iR/\ell)}{J_0^2(iR/\ell)}\right] J_0(ir/\ell) \right\} \frac{\Delta T}{L}, \tag{29}$$

wherein $J_1(z)$ is the first-order cylindrical Bessel function. By the way, we used the relation $dJ_0(cz)/dz = -cJ_1(cz)$, where $c$ is generic constant. Since we are assuming $R$ comparable to $\ell$, then $q_w$ depends on the radial distance from the wall in Eq. (29). Whenever $R \ll \ell$ the wall contribution $q_w$ will be constant.

Integrating Eqs. (28) and (29) across the transversal section, one finally may get that the effective thermal conductivity is [104]

$$\kappa_{\text{eff}}(\text{Kn}) = \kappa_0 \left\{ 1 - 2\,\text{Kn} \left[\frac{J_1(i/\text{Kn})}{J_0(i/\text{Kn})}\right]^2 \left[\frac{J_0(i/\text{Kn})}{iJ_1(i/\text{Kn})} + C\right] \right\}, \tag{30}$$

where the Knudsen number is defined as $\text{Kn} = \ell/R$. In very rarefied situations (that is, when $\text{Kn} \gg 1$), the heat flux $q$ may be neglected in Eq. (27), namely, one may use the one-dimensional version of Eq. (6), and the effective thermal conductivity (37a) reduces to [2]

$$\kappa_{\text{eff}}(\text{Kn}) = \frac{\kappa_0}{8\,\text{Kn}^2}(1 + 4C\,\text{Kn}). \tag{31}$$

It is easy to see that in the limit of very high Kn, the predicted effective thermal conductivity decreases again linearly in terms of $\text{Kn}^{-1}$, along with Eq. (20).

## 3. Roughness dependence of the effective thermal conductivity

In this section we give a deeper insight on the structure of the walls. A sketch of such a structure is represented in Fig. 1.

We consider that the roughness of the wall is described by two parameters (see Fig. 1): $\Delta$ which is the root-mean square value (rms) of the roughness fluctuations, and $D$ which is the average distance between roughness peaks [40]. In terms of these parameters in Ref. [102] the coefficients $C$ and $\alpha$ in Eqs. (9) have been modeled as

$$\begin{cases} C = C'\left(1 - \dfrac{\Delta}{D}\right), \\ \alpha = \alpha' \dfrac{\Delta}{D}, \end{cases} \tag{32}$$

where $C'$ and $\alpha'$ are numerical dimensionless functions, dependent on temperature, but independent on $\Delta$ and $D$. Indeed, when $\Delta/D \to 0$ (or in the limit case when $\Delta = 0$), no backscattering is expected, but only specular and diffusive scattering. Therefore $\alpha \to 0$ when $\Delta/D \to 0$. On the other side, when $D = \Delta$, the surface has no flat regions, but it is completely rough, in which case $C = 0$ is expected.

Here we have assumed the simplest dependence for $C$ and $\alpha$ on the ratio $\Delta/D$. Another interesting proposal may be found in Ref. [125]. The coefficients $C'$ and $\alpha'$ will depend on temperature because a surface is considered smooth (or rough) when the characteristic height $\Delta$ of the roughness is smaller (or higher) than the phonon wavelength which depends on temperature [102].

By using Eq. (6) (this means that we are assuming $R \ll \ell$), in terms of the Knudsen number, in Ref. [3] the following effective thermal conductivity has been calculated

$$\kappa_{\text{eff}} = \frac{\kappa_0}{8\,\text{Kn}^2}\left(1 + 4C\,\text{Kn} - 4\alpha\,\text{Kn}^2\right), \tag{33}$$

which becomes

$$\kappa_{\text{eff}}\left(\text{Kn}; \frac{\Delta}{D}\right) = \frac{\kappa_0}{8\,\text{Kn}^2}\left(1 + 4C'\,\text{Kn}\right) - \frac{\kappa_0}{2\,\text{Kn}}\left(\frac{\Delta}{D}\right)\left(C' + \alpha'\,\text{Kn}\right), \tag{34}$$

once the assumptions (32) for $C$ and $\alpha$ are made. In Refs. [55, 77, 83] the effective thermal conductivity for smooth and rough Si nanowires of different cross section has been experimentally obtained. In the case of nanowires at 100 K ($\kappa_0 = 884\,\text{Wm}^{-1}\text{K}^{-1}$, and $\ell_{\text{Si}} = 557\,\text{nm}$) the results of Tabs. 2 and 3 follow from Eq. (34) in the case that $C' = 0.46$ and $\alpha' = 0.08$. These values for $C'$ and $\alpha'$ have been obtained in Ref. [102] in empirical way. Those results fit reasonably well experimental data taken from Refs. [55, 77, 83]. It turns out that the effective thermal conductivity results to be lowered by the roughness.

In particular, in Tab. 2 smooth-walled nanowires (i.e., $\Delta = 0\,\text{nm}$) have been analyzed so that only specular and diffusive scattering is considered (i.e., $\alpha = 0$ in Eq. (33)). It is seen that the influence of boundaries, as expressed by $C$, is extremely important, and that the only use of the Guyer-Krumhansl equation without complementing it with the constitutive equations (9) (i.e., $C = 0$ in Eq. (33), too) does not provide a satisfactory description of the effective thermal conductivity in the case of high Kn, namely, if $\ell \gg R$.

***Table 2.*** Effective thermal conductivity in silicon nanowires at 100 K in the presence of only specular and diffusive scattering (i.e., $\alpha = 0$). Comparison between experimental data (taken from Refs. [77]), the results predicted by Eq. (34). The results for $C' = 0$, instead, follow directly from the Guyer-Krumhansl equation in the case of high Kn, without using the constitutive equations (9).

| | Experimental data | $C' = 0.46$ | $C' = 0$ |
|---|---|---|---|
| $R$ [nm] | $\kappa_{\text{eff}}$ [$\text{Wm}^{-1}\text{K}^{-1}$] | $\kappa_{\text{eff}}$ [$\text{Wm}^{-1}\text{K}^{-1}$] | $\kappa_{\text{eff}}$ [$\text{Wm}^{-1}\text{K}^{-1}$] |
| 37 | 14 | 13.62 | 0.47 |
| 56 | 23 | 20.87 | 1.12 |
| 115 | 45 | 45.46 | 4.74 |

In Tab. 3, instead, rough-walled nanowires have been analyzed ($\Delta = 3\,\text{nm}$ and $D = 6\,\text{nm}$) so that backscattering is taken into account. The results predicted by Eq. (34) are still in agreement with the results which we inferred from Refs. [55, 83] at 100 K.

***Table 3.*** Effective thermal conductivity in silicon nanowires at 100 K in the presence of backscattering ($\Delta = 3\,\text{nm}$, and $D = 6\,\text{nm}$). Comparison between the approximate experimental data inferred from Refs. [55, 83] and the results predicted by Eq. (34).

| | Experimental data | $C' = 0.46$ & $\alpha' = 0.08$ |
|---|---|---|
| $R$ [nm] | $\kappa_{\text{eff}}$ [$\text{Wm}^{-1}\text{K}^{-1}$] | $\kappa_{\text{eff}}$ [$\text{Wm}^{-1}\text{K}^{-1}$] |
| 97 | 3.85 | 2.42 |
| 115 | 5.75 | 6.89 |

In Ref. [101] (see Tabs. IV and V therein) comparison between experimental values and theoretical ones has been made for a wider range of temperature. The good agreement which can be found therein strengthens the importance of accounting for phonon-wall interactions.

If the hypothesis of high Knudsen number is relaxed, in the general case of a steady-state situation the condition $\mathbf{q} \ll \ell^2\nabla^2\mathbf{q}$ is not satisfied, and one should use the full steady-state version of Guyer-Krumhansl equation, namely,

Eq. (5). The solution of that equation is cumbersome in cylindrical geometry, but results may be easily derived for thin layers (refer to Fig. 2 for the system of coordinates). For this system, in Ref. [2] (see Eq. (18) therein) it has been derived that the bulk heat profile with a vanishing value at the walls (i.e., when $r = \pm h/2$) is given by

$$q_b(r) = -\kappa_0 \left[1 - \frac{e^{\frac{r}{l}} + e^{-\frac{r}{l}}}{e^{\frac{1}{2\,\mathrm{Kn}}} + e^{-\frac{1}{2\,\mathrm{Kn}}}}\right] \frac{\Delta T}{L}. \tag{35}$$

Once Eq. (9a) is assumed as constitutive equation for $\mathbf{q}_w$ and Eq. (35) is introduced into it, the wall contribution is obtained. When added to the bulk contribution (35), straightforward calculations allow to obtain the following effective thermal conductivity

$$\kappa_{\mathrm{eff}} = \kappa_0 \left[1 - \alpha - (2\,\mathrm{Kn} - C)\tanh\left(\frac{1}{2\,\mathrm{Kn}}\right)\right]. \tag{36}$$

Thus, it is seen that the strong influence of the boundaries on the effective thermal conductivity is well represented by the phonon-hydrodynamics approach at the condition to complement the Guyer-Krumhansl equation with the constitutive equations (9a).

## 4. Frequency dependence of the effective thermal conductivity

The thermal propagation in nanosystems under a frequency-dependent temperature gradient is interesting from the practical point of view, because nanodevices in computers are aimed to work at high frequencies, in order to maximize the speed of computing processing. The model presented in Ref. [103], directly based on second-order phonon hydrodynamics, allows a more intuitive description of phonon transport and of the role of phonon-wall collisions. As a further new feature it incorporates relaxational effects in the boundary constitutive equations too, in order to study their influence on the thermal conductivity. The analysis is restricted to short enough wires, in order to avoid the consideration of heat waves propagation. Thus, let us consider the following sinusoidal varying perturbations for the difference in temperatures (applied at the ends of the systems) and for the bulk heat flow:

$$\Delta T(\omega; t) = \delta \tilde{T} e^{i\omega t}, \tag{37a}$$

$$q_b(r; \omega; t) = \tilde{q}_{b,0} \left(\frac{R^2 - r^2}{4\ell^2}\right) e^{i\omega t}, \tag{37b}$$

where $\omega$ is the angular frequency of the perturbation. Equation (37a) considers that the temperature only depends on the longitudinal position, but is homogeneous across each transversal area. Equation (37b) for the perturbation of the flux, instead, assumes that the bulk heat-flow profile keeps essentially the parabolic form corresponding to the so-called Poiseuille phonon flow [2, 101], but with an amplitude changing periodically (see Fig. 6 for a qualitative sketch).

Indeed, combining the local balance of energy (4) with Eq. (1) and introducing in it Eqs. (37), in the limit of high Kn, in Ref. [103] by straightforward calculations it has been obtained

$$q_b(r; \omega; t) = \left(\kappa_0 + 2i\omega c\ell^2\right) \left[\frac{R^2 - r^2}{4\ell^2 + i\omega\tau(R^2 - r^2)}\right] \frac{\delta \tilde{T}}{L} e^{i\omega t} \tag{38}$$

for the unsteady bulk heat-flow profile. In view of the dynamical form of the bulk heat-flow contribution (38), in the same way let us suppose that the wall contribution is given by

$$q_w(\omega; t) = \tilde{q}_{w,0} e^{i\omega t}, \tag{39}$$

wherein $\tilde{q}_{w,0}$ can be obtained from the constitutive equation in Eq. (10) [103], namely,

$$\tau_w \dot{q}_w + q_w = C\ell \left(\frac{\partial q_b}{\partial r}\right)_{r=R} - \alpha\ell^2 \left(\frac{\partial^2 q_b}{\partial r^2}\right)_{r=R}. \tag{40}$$

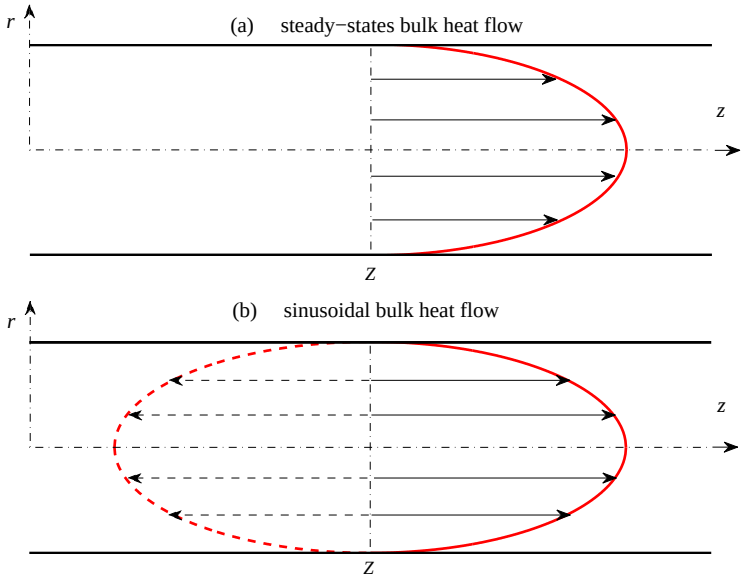


***Fig 6.*** Bulk heat-flow profile in nanowires given by Eq. (37b). The vertical dashed-dotted line $Z$ in each figure represents the transversal section, and the horizontal dashed-dotted line $z$ is the longitudinal axis. The bulk heat-flow profile is assumed to have a parabolic profile as in the steady Poiseuille phonon flow (Fig. 6a), but with a periodically dependent amplitude (Fig. 6b).

That constitutive equation has been also used in Ref. [66] to analyze heat waves and phonon-wall collisions in nanowires. In the case of smooth-walled nanowires (namely, when $\Delta/D = 0$) we take $\tau_w = R/\bar{c}$, with the average phonon velocity $\bar{c} = 8.43 \times 10^3\,\mathrm{m\,s^{-1}}$. For a nanowire with radius $R = 97\,\mathrm{nm}$, Eq. (11) (with $d = R$ therein) yields $\tau_w = 1.15 \times 10^{-2}\,\mathrm{ns}$. Finally, taking into account Eq. (38) for the bulk heat flow, and from the combination of Eqs. (39) and (40) for the frequency-dependent wall heat flow, the following form of the frequency-dependent effective thermal conductivity $\kappa_{\mathrm{eff}}$ may be obtained [103]:

$$\kappa_{\mathrm{eff}}(\omega;\mathrm{Kn}) = \mathrm{Re}\left\{\frac{Q_{\mathrm{tot}}}{\pi R^2}\frac{L'}{\delta T}\right\} = \frac{2\,\mathrm{Kn}^2}{\omega^2\tau^2}\left[\kappa_0 \ln\left(1+\frac{\omega^2\tau^2}{16\,\mathrm{Kn}^4}\right) - 4\omega c\ell^2 \arctan\left(\frac{\omega\tau}{4\,\mathrm{Kn}^2}\right)\right]$$
$$+\frac{2c\ell^2}{\tau}+\frac{C}{2\,\mathrm{Kn}}\left(\frac{\kappa_0+2\omega^2\tau_w c l^2}{1+\omega^2\tau_w^2}\right) - \frac{\alpha}{2\,(1+\omega^2\tau_w^2)}\left[\kappa_0\left(1+\frac{\omega^2\tau\tau_w}{\mathrm{Kn}^2}\right)+2\omega^2 c\ell^2\left(\tau_w-\frac{\tau}{\mathrm{Kn}^2}\right)\right]. \tag{41}$$

It is easy to observe that in the low-frequency limit (i.e., when $\omega\tau \to 0$), the frequency-dependent effective thermal conductivity (41) reduces to the value of the effective thermal conductivity in steady states, whereas in the high-frequency limit (i.e., when $\omega\tau \to \infty$) one has

$$\kappa_{\mathrm{eff}}(\mathrm{Kn}) = \frac{2c\ell^2}{\tau}\left\{1+\frac{1}{2}\frac{\tau}{\tau_w}\left[\frac{C}{\mathrm{Kn}}-\alpha\left(1-\frac{\tau}{\tau_w}\frac{1}{\mathrm{Kn}^2}\right)\right]\right\} - \frac{\alpha}{2}\frac{\kappa_0}{\mathrm{Kn}^2}\frac{\tau}{\tau_w}. \tag{42}$$

To illustrate explicitly the results arising from Eq. (42) we assume a rough-walled silicon nanowire with $R = 97\,\mathrm{nm}$. Then, in Fig. 7 and Fig. 8 we compare the behavior of the frequency-dependent effective thermal conductivity in terms of $\omega\tau$. We assumed again that the walls are characterized by $\Delta = 3\,\mathrm{nm}$ and $D = 6\,\mathrm{nm}$. In each figure, two different values of the temperature have been considered, i.e., $T = 30\,\mathrm{K}$ and $T = 50\,\mathrm{K}$ in Fig. 7, and $T = 100\,\mathrm{K}$ and $T = 150\,\mathrm{K}$ in Fig. 8. To obtain the specific heat per unit volume we use the classical Debye expression, namely, $c_v = \left(12\pi^4/5\right)(T/T_B)^3\left(G\varrho_{\mathrm{Si}}/M_{\mathrm{Si}}\right)$, with $\varrho_{\mathrm{Si}} = 2.33 \times 10^3\,\mathrm{Kg\,m^{-3}}$ being the mass density of silicon, $T_B = 645\,\mathrm{K}$ being the Debye temperature, $G = 8.31\,\mathrm{J\,K^{-1}\,mol^{-1}}$ being the gas constant, and $M_{\mathrm{Si}} = 28 \times 10^{-3}\,\mathrm{Kg\,mol^{-1}}$ being the molar mass. Moreover, the relaxation time $\tau_w$ has been estimated by using Eq. (11) and is $\tau_w = 1.14 \times 10^{-2}\,\mathrm{ns}$.

From the analysis of Fig. 7 and Fig. 8 it is possible to infer that the frequency-dependent effective thermal conductivity increases both for increasing temperature, and for increasing frequency $\omega$. For the sake of comparison, we consider also the behavior of the frequency-dependent effective thermal conductivity in a smooth-walled nanowire, namely, when $\alpha = 0$ in Eq. (41). By using the same parameters as above, these behaviors are plotted in Fig. 9 and Fig. 10. As it is possible to observe, the effective thermal conductivity is still increasing both for increasing frequency, and for increasing temperature. Moreover, as it is intuitive, the comparison between Figs. 7-10 shows that the presence of backscattering sensibly reduces the thermal conductivity.

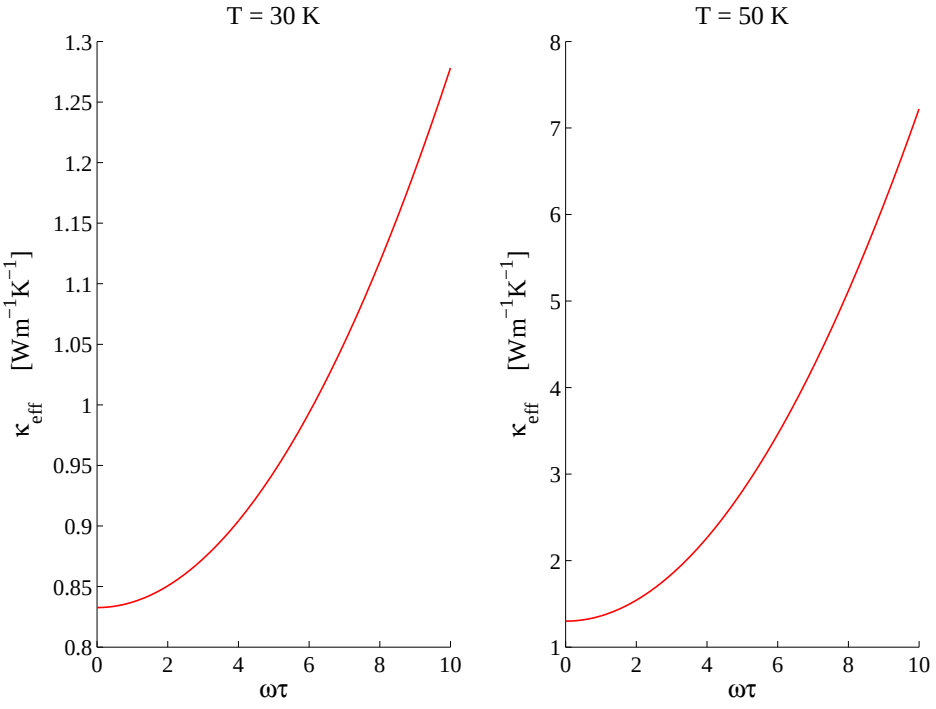


***Fig 7.*** Behavior of the frequency-dependent effective thermal conductivity (i.e., Eq. (41)) as a function of $\omega\tau$ in the presence of backscattering. Two different temperatures (i.e., $T = 30\,\mathrm{K}$ and $T = 50\,\mathrm{K}$) have been considered. The corresponding Knudsen numbers are, respectively, $\mathrm{Kn} = 168.6$ and $\mathrm{Kn} = 68.9$. The nanowire is made of silicon and has $R = 97\,\mathrm{nm}$, $\Delta = 3\,\mathrm{nm}$ and $D = 6\,\mathrm{nm}$. To get better visualization of results, different length scales for $\kappa_{\mathrm{eff}}$ at different temperatures have been used.

## 5. Size dependence of the figure-of-merit in thermoelectric rigid conductors

The conversion of heat current into electric current through thermoelectric effects, i.e., the direct conversion of temperature differences to electric voltage and vice-versa, offers a promising avenue in energy management [8, 10, 13, 36, 115]. Since a larger value of $ZT$ indicates a greater thermodynamic efficiency [72], the evaluation of $ZT$ is important for comparing the potential efficiency of devices using different materials. Indeed, the search of materials with high values of $Z$ is a hot topic of research [13, 23, 35, 72, 126], and nowadays the figure-of-merit of many materials has been explored [60, 91, 92]. To date, the best reported $ZT$ values are in the $2-3$ range, and one of the current tasks in design of nanostructured materials is to achieve $ZT \simeq 3$, or larger.

An interesting aspect of nanosystems is the possibility of an additional control of the transport coefficients by getting sizes comparable to the mfp $\ell$ of the different heat carriers (phonons, electrons, holes, etc.). Since the values of the mfps differ from each other, it is possible to reduce some coefficients while keeping the usual values for other ones. For instance, in nanowires it is expected that whenever the radius of the transversal section is comparable to (or smaller than) the phonon mfp, the phonon contribution to the thermal conductivity $\kappa_p$ will be reduced, leading to an increase of $Z$, according to Eq. (12). Furthermore, it is expected that the power factor $\epsilon^2\sigma_e$ would also increase as a result of the quantum confinement effects arising when a material is confined into a nanostructure [31, 90]. Thus, incorporating

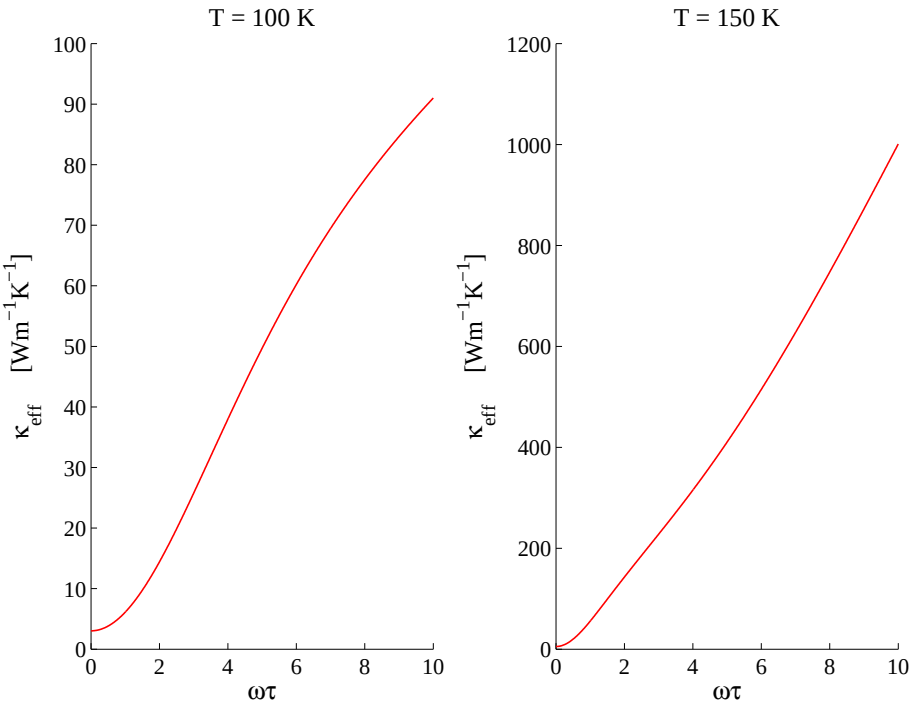


***Fig 8.*** Behavior of the frequency-dependent effective thermal conductivity (i.e., Eq. (41)) as a function of $\omega\tau$ in the presence of backscattering. Two different temperatures (i.e., $T = 100\,\mathrm{K}$ and $T = 150\,\mathrm{K}$) have been considered. The corresponding Knudsen numbers are, respectively, $\mathrm{Kn} = 5.7$ and $\mathrm{Kn} = 1.9$. The nanowire is made of silicon and has $R = 97\,\mathrm{nm}$, $\Delta = 3\,\mathrm{nm}$ and $D = 6\,\mathrm{nm}$. To get better visualization of results, different length scales for $\kappa_{\mathrm{eff}}$ at different temperatures have been used.

explicitly the effects of the several mfps is useful to study new strategies for the optimization of these effects [128].

We start to focus our attention on a cylindrical nanowire in a stationary state, with a transversal radius $R$ such that $(R < \ell_e, \ell_p)$, so that all the fluxes undergo the hydrodynamic regime. In this case, Eqs. (14) reduce to [108]

$$\nabla^2 \mathbf{q}^{(p)} = \frac{\kappa_p}{\ell_p^2} \nabla T, \tag{43a}$$

$$\nabla^2 \mathbf{q}^{(e)} = \frac{1}{\ell_e^2} \left[ \left( \kappa_e + \epsilon \Pi \sigma_e \right) \nabla T - \Pi \sigma_e \mathbf{E} \right] - 2 \nabla \left( \mathbf{E} \cdot \mathbf{I} \right), \tag{43b}$$

$$\nabla^2 \mathbf{I} = \frac{\sigma_e}{\ell_e^2} \left( \epsilon \nabla T - \mathbf{E} \right). \tag{43c}$$

Then, we obtain the following parabolic longitudinal profiles [108]:

$$q^{(p)}(r) = \kappa_p \frac{\Delta T}{L} \frac{\left( R^2 - r^2 \right)}{4 \ell_p^2}, \tag{44a}$$

$$q^{(e)}(r) = q^{(e,\Delta T)}(r) + q^{(e,\mathrm{E})}(r) = \left[ \left( \kappa_e + \epsilon \Pi \sigma_e \right) \frac{\Delta T}{L} + \Pi \sigma_e \mathrm{E} \right] \frac{\left( R^2 - r^2 \right)}{4 \ell_e^2}, \tag{44b}$$

$$I(r) = I^{(\Delta T)}(r) + I^{(\mathrm{E})}(r) = \sigma_e \left( \epsilon \frac{\Delta T}{L} + \mathrm{E} \right) \frac{\left( R^2 - r^2 \right)}{4 \ell_e^2}, \tag{44c}$$

arising from Eqs. (43) with the assumptions of vanishing values of the corresponding quantities at the walls, namely, by supposing that $q^{(e)}(R) = 0$, $q^{(p)}(R) = 0$ and $I(R) = 0$.

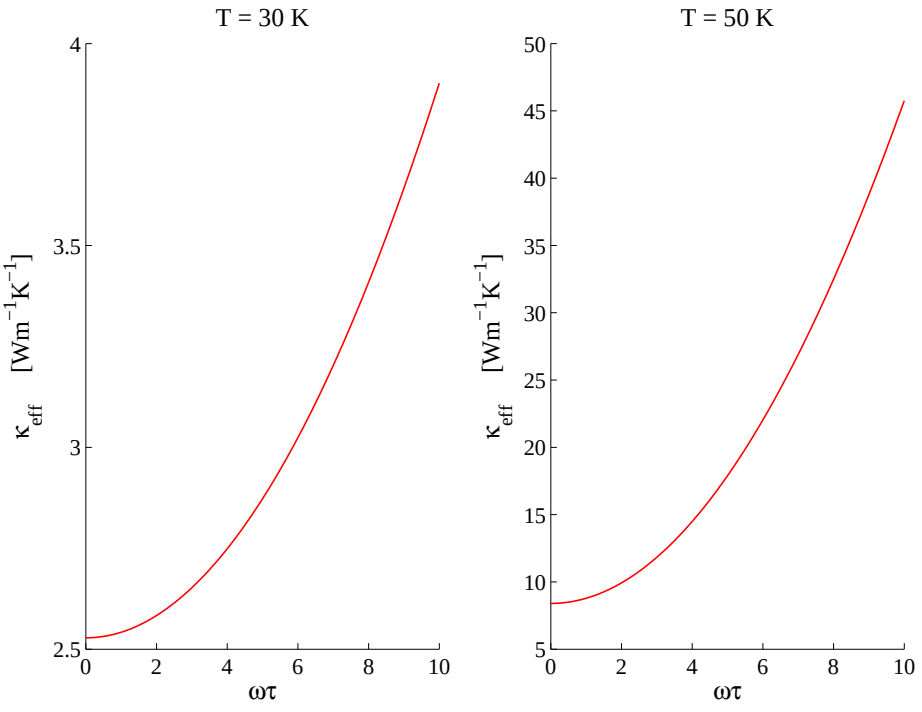


***Fig 9.*** Behavior of the frequency-dependent effective thermal conductivity (i.e., Eq. (41)) as a function of $\omega\tau$ in absence of backscattering. Two different temperatures (i.e., $T = 30\,\mathrm{K}$ and $T = 50\,\mathrm{K}$) have been considered. The nanowire is made of silicon and has $R = 97\,\mathrm{nm}$. To get better visualization of results, different length scales for $\kappa_{\mathrm{eff}}$ at different temperatures have been used.

Now, let us assume [108]

$$q^{(e)}(r) = q_{\mathrm{b}}^{(e)}(r) + q_{\mathrm{w}}^{(e)}, \tag{45a}$$

$$q^{(p)}(r) = q_{\mathrm{b}}^{(p)}(r) + q_{\mathrm{w}}^{(p)}, \tag{45b}$$

$$I(r) = I_{\mathrm{b}}(r) + I_{\mathrm{w}}, \tag{45c}$$

together with the following constitutive equations for the fluxes on the wall:

$$q_{\mathrm{w}}^{(e)} = C_e \ell_e \left| \frac{\partial q_{\mathrm{b}}^{(e)}}{\partial r} \right|_{r=R}, \tag{46a}$$

$$q_{\mathrm{w}}^{(p)} = C_p \ell_p \left| \frac{\partial q_{\mathrm{b}}^{(p)}}{\partial r} \right|_{r=R}, \tag{46b}$$

$$I_{\mathrm{w}} = C_e \ell_e \left| \frac{\partial I_{\mathrm{b}}}{\partial r} \right|_{r=R}, \tag{46c}$$

where $C_e$ plays the same role of $C_p$, namely, it is a non-negative numerical coefficient characterizing the wall. Moreover, $q_{\mathrm{b}}^{(e)}$, $q_{\mathrm{b}}^{(p)}$ and $I_{\mathrm{b}}$ represent the bulk values of the corresponding quantities, and are given by Eqs. (44).

In such a situation, under the hypotheses that $\mathbf{E}$, $\mathbf{I}$ and $\nabla T$ are first-order quantities and that second-order quantities are negligible, and that $\nabla T$ and $\mathbf{E}$ are homogeneous across each transversal section and along the nanowire, in Ref. [108] the authors get the following figure-of-merit:

$$Z = \frac{\epsilon^2 \sigma_e \left(1 + 4C_e \dfrac{\ell_e}{R}\right)}{\kappa_e \left(1 + 4C_e \dfrac{\ell_e}{R}\right) + \kappa_p \dfrac{\ell_e^2}{\ell_p^2} \left(1 + 4C_p \dfrac{\ell_p}{R}\right)}. \tag{47}$$

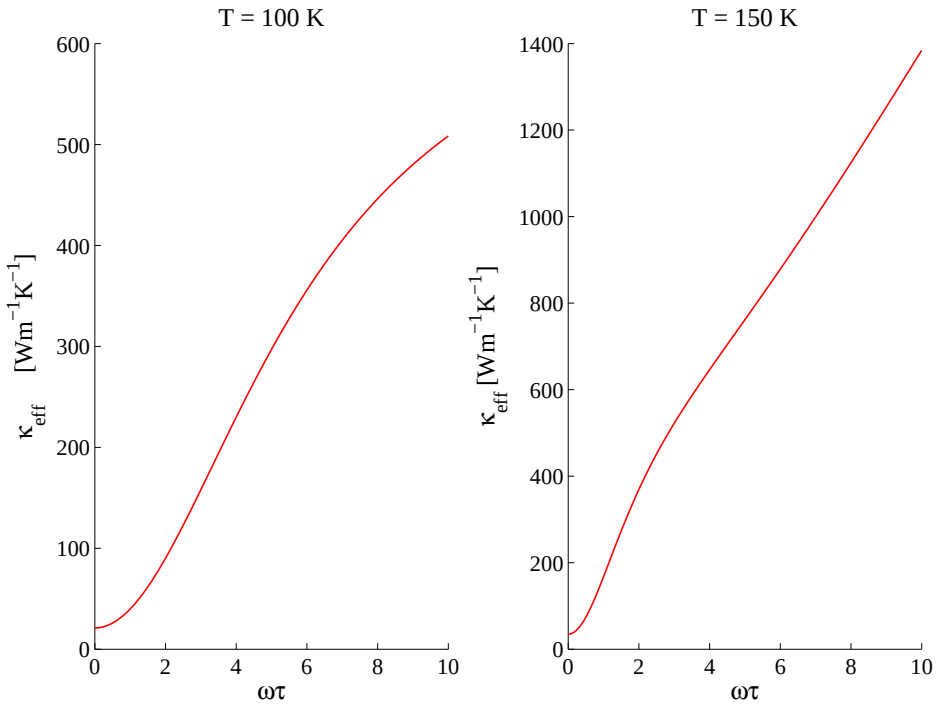


***Fig 10.*** Behavior of the frequency-dependent effective thermal conductivity (i.e., Eq. (41)) as a function of $\omega\tau$ in absence of backscattering. Two different temperatures (i.e., $T = 100\,\mathrm{K}$ and $T = 150\,\mathrm{K}$) have been considered. The nanowire at hand is made of silicon and has $R = 97\,\mathrm{nm}$. To get better visualization of results, different length scales for $\kappa_{\mathrm{eff}}$ at different temperatures have been used.

For very small $R$, the nondimensional ratios between the mfps and the radius become dominant in Eq. (47), and we have

$$Z = \frac{\epsilon^2 \sigma_e}{\kappa_e + \kappa_p \left(\frac{C_p}{C_e}\right)\left(\frac{\ell_e}{\ell_p}\right)}, \tag{48}$$

namely, in this case the modulation of $Z$ could come from the roughness of the walls, which will determine the relative values of $C_p$ and $C_e$. The presence of $C_p$ and $C_e$ in Eq. (48) reflects the importance of the interactions between phonons and walls, and between electrons and walls, as it would be expected on intuitive ground. In fact, for a given temperature, the ratio $\ell_e/\ell_p$ is fixed and its value depends on the material at hand. However, Eq. (48) suggests that $Z$ can be changed by modeling the walls of the nanowire in such a way that the number of reflected electrons is different from the number of reflected phonons, i.e., varying the ratio $C_p/C_e$. This can be also observed from Fig. 11, which plots the behavior of $ZT$ in a $p$-doped nanosample of $Bi_2Te_3$ at 300 K as a function of the ratio $C_p/C_e$. The values of the material functions are taken by Ref. [52, 53] (refer to Tab. 4 for these values at room temperature) in the case of $Bi_2Te_3$ nanowires, which are often used in thermoelectric applications [93, 99].

***Table 4.*** Values of the material functions for a $p$-doped sample of $Bi_2Te_3$ at 300 K [52, 53].

| $\kappa_p$ [W m$^{-1}$ K$^{-1}$] | $\kappa_e$ [W m$^{-1}$ K$^{-1}$] | $\ell_p$ [m] | $\ell_e$ [m] | $c_v$ [Jm$^{-3}$K$^{-1}$] | $\sigma_e$ [$\Omega^{-1}$ m$^{-1}$] | $\epsilon$ [V °C$^{-1}$] |
|---|---|---|---|---|---|---|
| 1.6 | 2.4 | $3.0 \times 10^{-9}$ | $9.1 \times 10^{-10}$ | $1.2 \times 10^{6}$ | $2.0 \times 10^{5}$ | $2.0 \times 10^{-4}$ |

In particular, the analysis of Fig. 11 suggests that an enhancement of the figure-of-merit may be obtained when the number of reflected electrons is bigger than that of reflected phonons, i.e., the bigger $C_e$ than $C_p$, the higher $Z$.

In some applications the characteristic size $R$ may become bigger than the electrons' mfp, and one has $\ell_e < R < \ell_p$. In this situation we may assume the hydrodynamic regime for the phonon heat flux $\mathbf{q}^{(p)}$, whereas for the electron heat

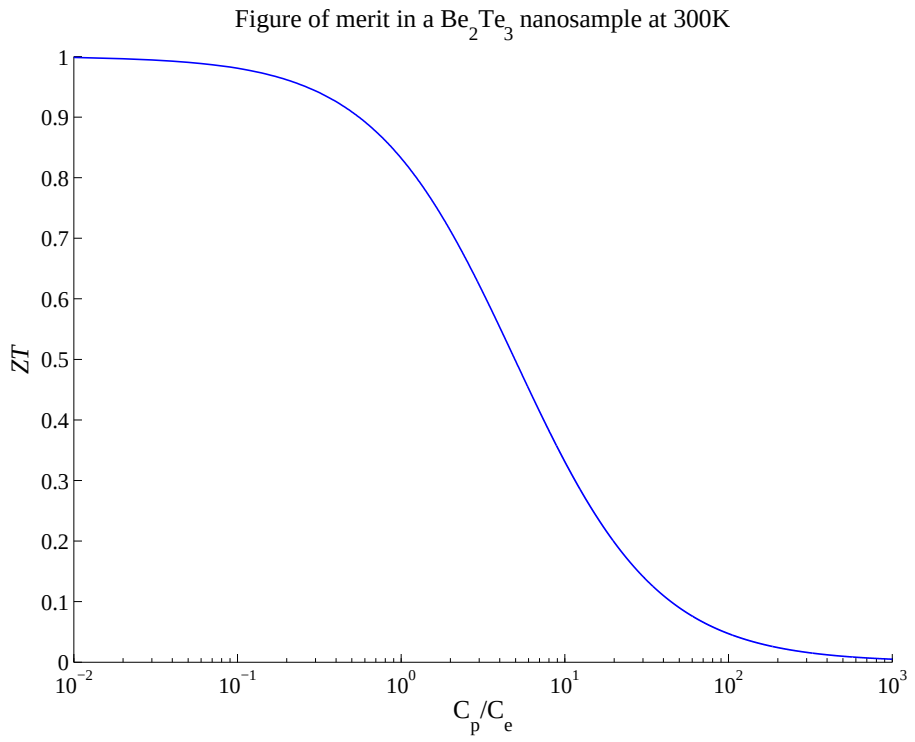


***Fig 11.*** Behavior of $ZT$, arising from Eq. (48), in a $p$-doped $Bi_2Te_3$ nanosample at 300 K as a function of the ratio $C_p/C_e$ in the case of $R < \ell_e, \ell_p$. The values of the material functions are taken from Tab. 4. In figure the $x$-axis is in a logarithmic scale.

flux $\mathbf{q}^{(e)}$ and the electric-current density $\mathbf{I}$ we have the usual resistive regime, which takes place when the second-order spatial derivatives of the flux can be neglected and the important term in the evolution equation is contributed by the flux itself. Then, Eqs. (14) become [108]

$$\nabla^2 \mathbf{q}^{(p)} = \frac{\kappa_p}{\ell_p^2} \nabla T, \tag{49a}$$

$$\mathbf{q}^{(e)} = -\left(\kappa_e + \epsilon \Pi \sigma_e\right) \nabla T + \Pi \sigma_e \mathbf{E}, \tag{49b}$$

$$\mathbf{I} = \sigma_e \left(\mathbf{E} - \epsilon \nabla T\right). \tag{49c}$$

If only the system (49) is used, without complementing it with the boundary constitutive equations, it turns out that the effective transport coefficients are:

$$\left(\kappa_e + \epsilon \Pi \sigma_e\right)_{\text{eff}} = \kappa_e + \epsilon \Pi \sigma_e, \tag{50a}$$

$$\left(\Pi \sigma_e\right)_{\text{eff}} = \Pi \sigma_e, \tag{50b}$$

$$\left(\kappa_p\right)_{\text{eff}} = \kappa_p \frac{R^2}{8\ell_p^2}, \tag{50c}$$

$$\left(\epsilon \sigma_e\right)_{\text{eff}} = \epsilon \sigma_e, \tag{50d}$$

$$\left(\sigma_e\right)_{\text{eff}} = \sigma_e. \tag{50e}$$

Owing to the formulae above, the following effective figure-of-merit $Z$ is easily derived:

$$Z = \frac{\epsilon^2 \sigma_e}{\kappa_e + \kappa_p \dfrac{R^2}{8\ell_p^2}}. \tag{51}$$

It explicitly shows the dependence of $Z$ on the transversal radius. For increasing values of the ratio $\ell_p/R$, from Eqs. (50c) it follows that $\kappa_p^{\text{eff}}$ decreases quadratically, so that from Eq. (51) we infer that $Z$ increases with respect to its bulk value and tends quadratically to the limit value $\epsilon^2\sigma_e/\kappa_e$. A similar behavior for the figure-of-merit as a function of the radius may be found in Ref. [52, 53] in the case of $Bi_2Te_3$ nanowires (refer to Tab. 4 for the values of the corresponding material functions at room temperature).

If, instead, we suppose that the phonon heat flux is $q^{(p)}(r) = q_{\text{b}}^{(p)}(r) + q_{\text{w}}^{(p)}$, where $q_{\text{w}}^{(p)}$ is the wall contribution to the heat flux, given by [108]

$$q_{\text{w}}^{(p)} = C_p \ell_p \left| \frac{\partial q_{\text{b}}^{(p)}}{\partial r} \right|_{r=R}, \tag{52}$$

we obtain the following expression for $(\kappa_p)_{\text{eff}}$

$$\left(\kappa_p\right)_{\text{eff}} = \kappa_p \frac{R^2}{8\ell_p^2} \left(1 + 4C_p \frac{\ell_p}{R}\right). \tag{53}$$

In such a situation $Z$ becomes [108]

$$Z = \frac{\epsilon^2\sigma_e}{\kappa_e + \kappa_p \left(\frac{C_p}{2}\right)\left(\frac{R}{\ell_p}\right)}. \tag{54}$$

As it is possible to observe, the figure-of-merit still depends on $R$. For increasing values of the ratio $\text{Kn}_p = \ell_p/R$, $Z$ still increases and tends to the limit value $Z_{\text{lim}} = \epsilon^2\sigma_e/\kappa_e$, but with a linear behavior, as it can be seen from Fig. 12, wherein the behavior of $ZT$, as a function of the ratio $\text{Kn}_p$, is plotted for different values of the numerical coefficient $C_p$ in the case of a nanosample made of a $p$-doped $Bi_2Te_3$ at 300 K. Figure 12 points out the relevance of the coefficient $C_p$, describing the phonon-wall collisions. If the walls are rough [55], $C_p$ will be small and the predicted $Z$ will exhibit an enhancement, with respect to the prediction of Eq. (51) ($C_p = 0$ in Fig. 12). Let us note that the ratio $\text{Kn}_p$ can be modified both by varying $R$, and by varying the temperature, since the mfps are temperature dependent.

## 6. Pore-size dependence of the effective thermal conductivity in porous silicon

The experimental results on pSi show that its thermal conductivity is strongly related to the pore size at a given total porosity [37–39, 110]. Since an increasing porosity may deteriorate the electron transport properties [5, 75], it would be advantageous if its effective thermal conductivity could be controlled by the volume fractions, as well as the characteristic size of the pores.

To achieve a simple model of porosity in Refs. [3, 107] the authors use classical hydrodynamics and consider a rigid sphere, with radius $r$, moving with a given speed $\mathbf{v}$ in a viscous fluid with shear viscosity $\eta$. Due to the viscosity, a drag-force $\mathbf{D}_\eta$, acting on the external surface of the sphere, is present. If the Reynolds number $\text{Re} = vr/\nu$, $\nu$ being the kinematic viscosity, is smaller than the unit, this force can be estimated by the Stokes formula, i.e.,

$$\mathbf{D}_\eta = 6\pi\eta r\mathbf{v}. \tag{55}$$

The dependence of $\mathbf{D}_\eta$ on $\mathbf{v}$ becomes quadratic when the Reynolds number is bigger than 1, i.e., when $\mathbf{v}$ gets sufficiently high values. However, in what follows only the linear dependence will be considered. When the flow becomes rarefied, the effects of a slip flow on the external surface of the sphere must also be taken into account. This means that the aforementioned drag force is reduced. In particular, when the sphere size is less than (or comparable with) the molecular mfp, Eq. (55) has to be modified according to the so-called Cunningham correction factor [32]

$$\Gamma_1 = 1 + 2\frac{l}{r}\left(1.257 + 0.4e^{-1.1r/l}\right), \tag{56}$$

such that $\mathbf{D}_\eta = 6\pi\eta r\mathbf{v}/\Gamma_1$, where $l$ is the molecular mfp, which accounts for the rarefaction effects: the higher $l$, the smaller $\mathbf{D}_\eta$. In the literature, other different proposals for this factor can be found [7, 85]. In particular situations, one may have several rigid spheres, instead of a single sphere, adsorbed in the gas flow. In such a case, the drag on each sphere changes [54, 69, 70, 96–98] and is given by $\mathbf{D}_\eta = 6\pi\eta r\mathbf{v}/(\Gamma_1\Gamma_2)$, where $\Gamma_2$ is a further correction factor.

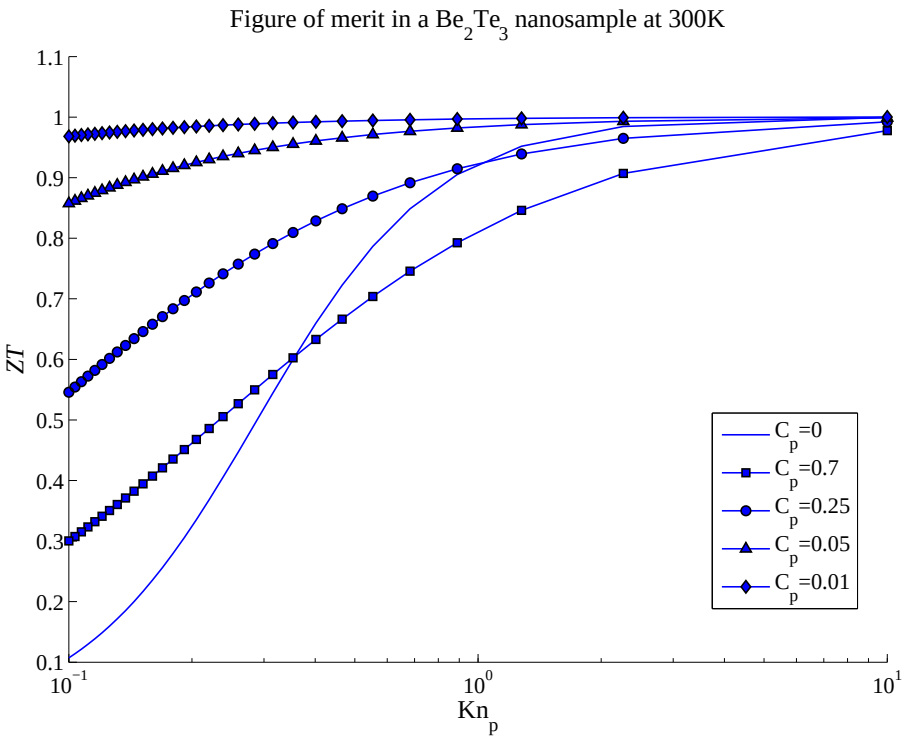


***Fig 12.*** Behavior of $ZT$ in a $p$-doped $Bi_2Te_3$ nanosample at 300 K as a function of the ratio $Kn_p$: comparison between Eq. (51) ($C_p = 0$ in figure) and Eq. (54) ($C_p \neq 0$ in figure) in the case of $\ell_e < R < \ell_p$. Different orders of magnitude for $C_p$ have been taken into account, in order to explore the influence of the phonon-wall collisions on $Z$. Refer to Tab. 4 for the values of the material functions.

Considering a finite volume (which we suppose to be completely made of gas and spheres), it is possible to introduce the volume-fraction $\varphi$ corresponding to the spheres. Then, the correction factor $\Gamma_2$ is given by

$$\Gamma_2 = 1 - 1.76\sqrt[3]{\varphi} + \varphi \quad \text{(SCD)} \tag{57a}$$

$$\Gamma_2 = 1 - 1.79\sqrt[3]{\varphi} + \varphi \quad \text{(BCCD)} \tag{57b}$$

for a simple-cubic distribution (SCD) (that is, Eq. (57a)), or a body-centered cubic distribution (BCCD) (that is, Eq. (57b)). In the case of a random distribution of spheres (RD), instead, the correction factor $\Gamma_2$ is given by the Brinkman expression [14]

$$\Gamma_2 = \left(1 + \frac{3}{\sqrt{2}}\sqrt{\varphi}\right)^{-1} \quad \text{(RD)}. \tag{58}$$

In Refs. [3, 107] the thermal conductivity of pSi is analyzed by regarding it as a silicon solid matrix with inclusion of small insulating spheres (see Fig. 13 for a qualitative sketch) which are supposed to have the same radius $r$.

Suppose that heat is flowing through the system. The flow of phonons is hindered and reduced by the insulating spheres. Therefore, a nonstandard thermal-drag force $\mathbf{T}_p$, due to the porosity, is acting on each single insulating sphere. Thus, in the phonon-hydrodynamic approach, for moderate values of $\mathbf{q}$, we may use the results above to estimate this force. We get so

$$\mathbf{T}_p = \frac{6\pi r \ell^2}{\Gamma_1 \Gamma_2 \kappa_0}\mathbf{q}, \tag{59}$$

where $\Gamma_1$ and $\Gamma_2$ are given, respectively, by Eq. (56) and Eqs. (57) (or Eq. (58) depending on the distribution), once the molecular mfp $l$ is replaced by the phonon mfp $\ell$, as well as $\varphi$ is replaced by $\phi$. It is understood that in Eq. (59) $\ell$ and

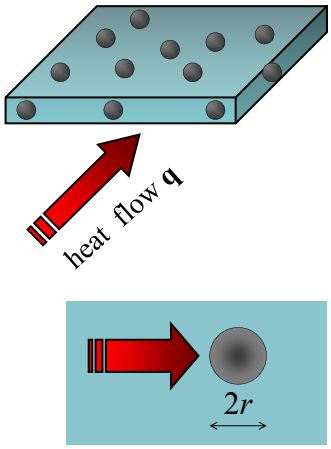


***Fig 13.*** Sketch of a pSi sample. The pores are considered as insulating spheres absorbed in a silicon solid matrix. The pores may be randomly distributed (RD) in the matrix (as in the picture), or have a periodic distribution (SCD, or BCCD). For the sake of simplicity, we suppose that all pores have the same radius equal to $r$. In figure the dimensions of the pores have been emphasized, in order to see easily the presence of the pores. The arrow in the figure stands for the heat flux.

$\kappa_0$ refer to silicon. Furthermore, in the presence of a flow through a medium, the standard thermal-drag force

$$\mathbf{T}_s = \frac{V}{\kappa_0 f(\phi)}\mathbf{q} \tag{60}$$

where $V$ is the volume of the system, has to be taken into account as well. Thus, if $N$ is the number of the insulating spheres, the resultant thermal-drag force is $\mathbf{T}_r = N\mathbf{T}_p + \mathbf{T}_s$. Since $\mathbf{T}_r$ balances the total driving thermal-force $V\nabla T$, due to the applied temperature gradient, we have

$$\left[\frac{6\pi N \ell^2 r}{\Gamma_1\Gamma_2} + \frac{V}{f(\phi)}\right]\frac{\mathbf{q}}{\kappa_0} = V\nabla T. \tag{61}$$

Since all the spheres have the same radius, in Eq. (61) we may explicit $N$ in terms of the porosity $\phi$, as $N = V/(\phi V_s)$, where $V_s = (4/3)\,\pi r^3$ is the volume of a single sphere. This way, straightforward calculations allow to obtain the following effective thermal conductivity [3]:

$$\kappa_{\text{eff}} = \frac{|\mathbf{Q}|}{A|\nabla T|} = \frac{\kappa_0}{\dfrac{1}{f(\phi)} + \dfrac{9}{2}\phi\dfrac{\text{Kn}^2}{\Gamma_1\Gamma_2}}, \tag{62}$$

where we have considered that $\mathbf{Q} = A\mathbf{q}$ is the total heat flux, $A$ being the transversal area (perpendicular to the direction of propagation of the heat flux), and $\text{Kn} = \ell/r$ is the Knudsen number. Looking at the denominator of Eq. (62), it is possible to distinguish clearly two different contributions: the first one related to the function $f(\phi)$ which accounts for the porosity, and the second one related to the Knudsen number Kn which is related, instead, to the characteristic size of the pores. For low values of Kn Eq. (62) reduces to Eq. (15). In Ref. [3], in the case of a random distribution of the pores, the authors have shown a good agreement between the experimental data and Eq. (62) when $f(\phi) = (1-\phi)^3$.

In Tab. 5 we report the experimental data for the thermal conductivity of pSi at the room temperature, for different porosity and pores' radii. In the same table, also the theoretical results, following from the relation $\kappa_{\text{eff}} = \kappa_0(1-\phi)^3$, are quoted. This way the importance of accounting for the role of the pores radius in the theoretical predictions may be enlighten.

In Tab. 6, instead, we show the theoretical results predicted by Eq. (62) for different internal distributions of the pores and for the same cases as in Tab. 5.

**Table 5.** Experimental results on the thermal conductivity of amorphous Si for different porosities $\phi$ and pores' radius $r$ at $T = 300\,\mathrm{K}$. In the same table, the theoretical data following from the relation $\kappa_{\mathrm{eff}} = \kappa_0 (1-\phi)^3$ are quoted, too.

| Source | $\phi$ [%] | $r$ [nm] | $\kappa_{\mathrm{eff}}$ [$\mathrm{Wm^{-1}K^{-1}}$] Experimental | $\kappa_{\mathrm{eff}}$ [$\mathrm{Wm^{-1}K^{-1}}$] Theoretical |
|---|---|---|---|---|
| Ref. [11] | 60 | 10 | 2 – 5 | 9.47 |
| Ref. [43] | 64 | 2 | 0.20 | 6.91 |
| Ref. [43] | 71 | 2 | 0.14 | 3.61 |
| Ref. [43] | 79 | 3 | 0.06 | 1.37 |
| Ref. [43] | 89 | 5 | 0.04 | 0.19 |

**Table 6.** Theoretical results on the thermal conductivity of pSi obtained from Eq. (62). Different internal distributions of the pores (SCD, BCCD and RD), different porosities $\phi$ and pores' radius $r$ have been analyzed. The sample is supposed at 300 K. At that temperature, for silicon one has $\ell = 40\,\mathrm{nm}$ and $\kappa_0 = 148\ \mathrm{Wm^{-1}K^{-1}}$.

| Source | $\phi$ [%] | $r$ [nm] | $\kappa_{\mathrm{eff}}$ [$\mathrm{Wm^{-1}K^{-1}}$] Eq. (62) – SCD | $\kappa_{\mathrm{eff}}$ [$\mathrm{Wm^{-1}K^{-1}}$] Eq. (62) – BCCD | $\kappa_{\mathrm{eff}}$ [$\mathrm{Wm^{-1}K^{-1}}$] Eq. (62) – RD |
|---|---|---|---|---|---|
| Ref. [11] | 60 | 10 | 3.41 | 2.89 | 6.13 |
| Ref. [43] | 64 | 2 | 0.92 | 0.73 | 2.17 |
| Ref. [43] | 71 | 2 | 0.83 | 0.71 | 1.56 |
| Ref. [43] | 79 | 3 | 0.74 | 0.69 | 0.98 |
| Ref. [43] | 89 | 5 | 0.18 | 0.18 | 0.18 |

In Fig. 14 we plot the behavior of the ratio of $\kappa_{\mathrm{eff}}$ to $\kappa_0$ at the room temperature and for two given values of porosity ($\phi = 0.3$ and $\phi = 0.6$), as a function of Kn, in the cases of SCD, BCCD and RD of the pores. In the same figure the effective thermal conductivity predicted by Eq. (15) is plotted as well. For the sake of computation, we assume $f(\phi) = (1-\phi)^3$ [80, 114]. However, the qualitative behaviors are independent of this choice. Let us explicitly note that Eq. (62) does not aim to be an exact formula, but it only provides an estimation which can be used as a preliminary step toward a phenomenological way to describe the effects of the pores' size on the thermal conductivity.

As it is possible to infer from Fig. 14, for increasing Kn the effective thermal conductivity of pSi decreases whatever the internal distribution of the pores is. In particular, the reduction in $\kappa_{\mathrm{eff}}$ seems to be rather strong, and only partly reduced by a random distribution of the pores.

Both from Tab. 6 and Fig. 14 it follows that, for a given porosity, the BCCD of the internal pores seems to be the best combination whenever pSi is used as device isolation in integrated circuits.

The results above are strictly related to the correction factor $\Gamma_1$, which accounts for particles-wall interactions. It has been expressed through Eq. (56), and is well-known in literature as the Cunningham factor [32]. Indeed, Eq. (56) is valid in the case of a smooth sphere with diffusive particles-wall collisions. When the radius of the sphere is comparable to the particles mfp, the wall roughness, as well as the wall heat flux, may be especially relevant [107] (see Fig. 15 for a sketch of the roughness of the pore wall).

If the assumptions (32) are made about the coefficients $C$ and $\alpha$, by using the results of Ref. [7], we may calculate the correction factor $\Gamma_1$ corresponding to this new situation. When $r \approx \ell$ we have that it would be no longer given by Eq. (56), but by the following expression:

$$\Gamma_1 = \frac{1 + 2C\dfrac{\ell}{r}}{1 + 3C\dfrac{\ell}{r} + \dfrac{3\alpha}{\pi}\dfrac{\ell^2}{r^2}}, \tag{63}$$

where $C$ and $\alpha$ are now suitable coefficients which may depend both on the radius of the pores, and on the roughness of the pores [107]. Since currently we are aware of experimental data for rough-walled pSi, Eq. (63) cannot be used for

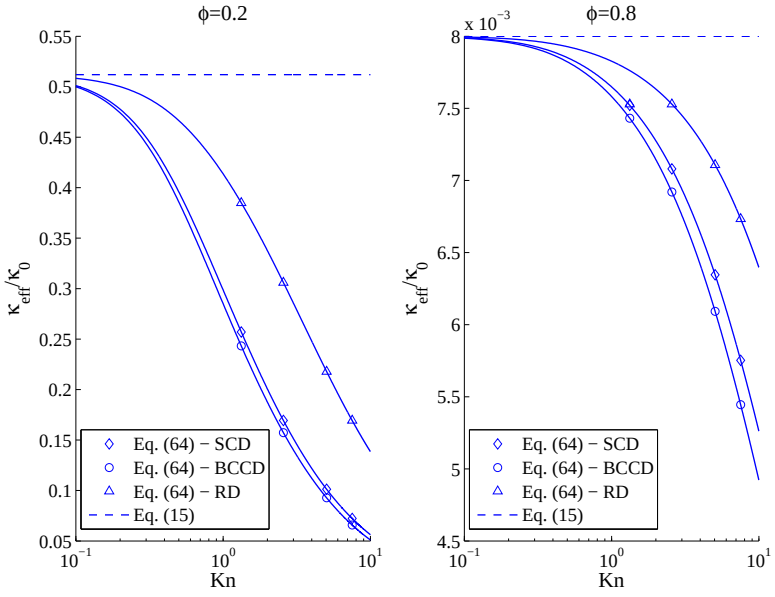


***Fig 14.*** Behavior of the ratio between $\kappa_{\text{eff}}$ and $\kappa_0$ as a function of Kn at $T = 300\,\text{K}$ ($\kappa_0 = 148\,\text{Wm}^{-1}\text{K}^{-1}$, $\ell = 40 \times 10^{-9}\,\text{m}$), arising from Eq. (62). Two different values of the porosity have been chosen, namely, $\phi = 0.2$ and $\phi = 0.8$. Moreover, for each value of $\phi$, the SCD, BCCD and RD of the pores have been considered. For the sake of comparison, in Fig. 7 also the behavior predicted by Eq. (15) is shown. Different length-scales have been used in figure.

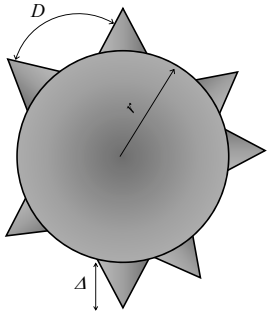


***Fig 15.*** Pore with rough wall. The roughness may be described by the roughness height ($\Delta$), and the separation of neighboring roughness peaks ($D$). Whenever a particle hits a peak, it may be reflected backward. Otherwise it is reflected in a diffusive or in a specular way.

the correction factor $\Gamma_1$ in order to evaluate the corresponding effective thermal conductivity. However, the increasing interest in pSi is fostering several experiments on its thermal properties. Thus, the knowledge in this area is in progress, and Eq. (63) may constitute the starting point of future research.

## 7. Open problems for future research

Finally, let us give an overview of some open problems, which deserve consideration for future research.

The temperature dependence of the boundary constitutive equation for $\mathbf{q}_w$ in phonon hydrodynamics follows from the experimental observations of the temperature dependence of the effective thermal conductivity of smooth and rough nanowires. A deep interpretation of this dependence should be based on detailed consideration of phonon-wall interactions. Here, instead, we have presented a phenomenological approach, based on the interpretation of the observations and the analysis of very simple features of the wall geometry, characterized by the height $\Delta$ of the roughness peaks and

their average separation $D$. The relation between the most probable phonon wave-length $\lambda_{\text{phonon}}$ and $\Delta$ has not been investigated, although it is expected to have a direct influence on the backscattering coefficient $\alpha'$, whereas the relation between $\lambda_{\text{phonon}}$ and $D$ could be expected to have an influence on a resonance in the coefficients $C'$. Though the former seems consistent with the estimated behavior of $\alpha'(T)$, the latter is not so successful, requiring a deeper analysis, as it seems that the minimum separation between roughness peaks is more relevant than the average separation of peaks $D$. From the observed $\kappa_{\text{eff}}(T)$ we arrived to the behavior of $C'(T)$ and $\alpha'(T)$, as an exploration. The desirable aim, in contrast, should start from $C'(T)$ and $\alpha'(T)$, as obtained from a microscopic understanding of phonon-wall interactions, to predict $\kappa_{\text{eff}}(T)$. There is yet a long way to achieve this aim.

One of the conclusions which can be inferred by the results of Sec. 3 is that the roughness of the walls should indeed influence the propagation speed of the heat waves. Thus, this speed could be used as an experimental tool to study the properties of the phonon-wall collisions in nanowires whose walls are sufficiently well known, and once these collisions are sufficiently well-known, use this technique to explore the features of the walls from the speed of heat waves, complementing the usual steady-state measurements of effective thermal conductivity.

A further topic of future research could be the improvement of the boundary constitutive equation in Eq. (63) (especially regarding the form of the wall-parameters $C$ and $\alpha$), and the study of nonlinear effects on the effective thermal conductivity when an Oseen-like correction to Eq. (59) is introduced [41]. For each of these topics, an analogous analysis could be carried out for two-dimensional plates with cylindrical pores across them. These systems are much studied as models of phononic crystals, because in such a case, in contrast to three-dimensional situations, the pores may be easily controlled.

An important conclusion following from the results in Sec. 4, is that the relaxational effects, due to collisions with the walls and characterized by the relaxation time $\tau_{\text{w}}$, have also a relevant influence on the effective thermal conductivity. Thus, more detailed attention should be paid to these effects in the future. An interesting aspect could be to consider the consequences of the relaxation time $\tau_{\text{w}}$ on the entropy in the system. It is known that the relaxation time in the bulk equation implies a generalization of the nonequilibrium entropy by incorporating the heat flux as an independent variable in it [63]. Therefore, it is logical to expect that the relaxational term in Eq. (10) for the wall heat flux would ask for a generalized entropy, incorporating the slip heat flow as an independent variable in a surface contribution to the entropy. Surface contributions to the entropy are of interest in the applications of thermodynamics to systems with wall contributions to the dynamics [127]. A first step in this direction was recently taken by Jou *et al.* [65], in a variational formulation of the Guyer-Krumhansl equation with a surface contribution to the entropy. In that paper, the bulk term and the surface term in the entropy were separately treated. It would be of interest to combine both contributions in a more general way, to look for a closer relation between the coefficient in the nonlocal term in Eq. (1) and the terms in Eq. (10) for the slip flow term. As the role of $\tau_{\text{w}}$ is usually not considered in the frequency-dependent thermal conductivity, one should be cautious with these preliminary results, until the dynamical aspects of phonon collisions with the walls are better understood. Indeed, from Eq. (41) it is possible to observe that the effect of $\tau_{\text{w}}$ is stronger than that of $\tau$ itself. This is logical, because in the situation we are studying the collisions of the phonons against the walls are much more frequent than that with other phonons or of impurities in the bulk.

Though the results in Eq. (48) and (54) could be obtained also from usual kinetic theory with the Matthiessen rule for the collision times including collisions with the walls, the model equations (14) are not always equivalent to a Fourier law and Ohm law, with size-dependent effective conductivities. Indeed, in axial geometries (as for example when heat and electric current flow radially away from a hot to a cold concentric cylinders) Eqs. (14) are not equivalent to effective Fourier and Ohm laws [106], but they predict different effects, which should be explored in the future.

Finally, we emphasize that an alternative approach to the problem of phonon-wall collisions is to incorporate the effect of these collisions directly into the microscopic form of the thermal conductivity [49, 50]. This is a satisfactory microscopic approach. However, our aim here was to review the possible applications of generalized phenomenological heat transport equations allowing for an explicit consideration of nonlocal effects and wall effects. A different approach beyond this line is that of the so-called thermomass theory [18, 34, 46, 47, 118, 119, 124], in which the heat-transfer process is regarded as a gas-like collection flowing in a medium due to a thermomass-pressure gradient. This flow is made by massive quasi-particles of heat carriers, i.e., the thermons [48, 123], whose mass may be calculated from the Einstein's mass-energy equation. In gases or liquids, the thermons are attached to the atoms or the molecules. In solids, instead, the thermons will be the phonon gas for crystals, or the electron gas for pure metals, or both of them for most of other solids. Since in this representation heat conduction is due to the motion of thermons, the continuity and momentum equations can be written as in fluid mechanics, and their combination yields the following evolution equation

for the heat flux [100, 119]:

$$\tau_{tm}\dot{\mathbf{q}} - c_v \mathbf{L}\dot{\theta} + \nabla\mathbf{q}\cdot\mathbf{L} + \kappa_0\left(1 - \mathrm{M}_{\mathrm{H}}^2\right)\nabla\theta + \mathbf{q} = 0, \tag{64}$$

wherein $\tau_{tm}$ is the relaxation time [34, 124] in the thermomass theory given by

$$\tau_{tm} = \frac{\kappa_0\rho}{2\gamma c_v^2 T},$$

$\gamma$ being the Grüneisen constant and $\Theta$ is the absolute temperature. Moreover in Eq. (64) $\mathbf{L}$ means a length vector (namely, the characteristic length of heat conduction [124]) given as $\mathbf{L} = \mathbf{q}\lambda\rho/\left[2\gamma c_v\left(c_v\theta\right)^2\right]$, and $\mathrm{M}_{\mathrm{H}} = q\sqrt{\rho}/\left(c_v\theta\sqrt{2\gamma c_v\theta}\right)$, $q$ being the modulus of the heat-flux vector, stands for a dimensionless number, less than unity, which is also called thermal Mach number of the drift velocity relative to the thermal-wave speed in the phonon gas [47, 119]. An interesting result is that Eq. (64) introduces a nonlinear thermal conductivity $\kappa_0\left(1 - \mathrm{M}_{\mathrm{H}}^2\right)$, which implies an upper bound for the heat flux for increasing temperature gradient. When compared to Eq. (1), Eq. (64) incorporates nonlinear effects (for instance the second and third terms therein) which do not appear in Eq. (1), or a heat-flux dependence of the thermal conductivity (i.e., the term in $\mathrm{M}_{\mathrm{H}}^2$ in Eq. (64)). In contrast, the equation characterizing the thermomass theory lacks the term in Laplacian of the heat flux appearing in Eq. (1). This is the reason why Eq. (64) does not pay so much attention to a slip heat flux along the walls. In spite of their differences, Eq. (1) and (64) may be fused into a single equation by incorporating the Laplacian term in the heat flux to Eq. (64), or, alternatively, by incorporating the nonlinear terms in Eq. (1). The consequences of such generalized equation, joining the efforts of phonon hydrodynamic model and thermomass theory, have not yet been explored in detail, but effort is being made along this line in Refs. [29, 30, 105].

Equation (64) has some valuable properties: it incorporates information on the characteristic length of the system, and accounts for nonlinear phenomena characterizing heat transport at the nanometric length scale. Moreover, it contains the convective term $\nabla\mathbf{q}\cdot\mathbf{q}$, allowing to study the stability of the heat flow by the methods of classical hydrodynamics [30], whenever the heat flux is negligible with respect to its spatial derivatives, as in nanosystems [2]. Therefore, in that phenomenological context, the analysis of the geometrical dependence of the effective heat conductivity may be a useful benchmark for the comparison of the several approaches to phonon heat transport.

The analysis of the thermodynamic consequences of nonlocal terms is not restricted to modifications in the entropy, but also in the entropy flux (see, for instance, Ref. [61] for a short didactical presentation). However, up to now, the explicit form of the entropy flux in the presence of nonlocal effects and its physical consequences have not been explored in depth. This could be useful to give a further perspective on thermodynamic restrictions on boundary effects.

In the present review only the linear effects have been explored. However the same emphasis could be also put on nonlinear effects, by examining generalized equations which exhibit them in an explicit way, especially the terms which are nonlinear in the heat flux itself. In Ref. [105] it has been introduced the following generalized nonlinear evolution equation

$$\tau\dot{\mathbf{q}} + \mathbf{q}\cdot\left(\mu\nabla\mathbf{q} + \mu'\nabla^T\mathbf{q}\right) + \mathbf{q} = -\kappa_0\left(1 + \beta\mathbf{q}\cdot\mathbf{q}\right)\nabla T + \ell^2\left(\nabla^2\mathbf{q} + 2\nabla\nabla\cdot\mathbf{q}\right), \tag{65}$$

where $\beta$, $\mu$ and $\mu'$ are coefficients accounting for nonlinear effects. Whenever such coefficients vanish, Eq. (65) reduces to Eq. (1). In that paper, by Eq. (65), the physical consequences of the nonlinear terms in the effective thermal conductivity of short carbon nanotubes, in the thermal rectification in a troncoconical nanowire, and in the radial heat transport in thin layers, have been analyzed. Since the solution of Eq. (65) may be cumbersome, especially for the geometries considered in the previous sections, as a first approximation wall effects have been neglected in Ref. [105]. It would be interesting to apply the methodology presented here, by incorporating the heat flux at the wall into the overall heat flux, in situations in which Eq. (1) is substituted by Eq. (65), in order to investigate the simultaneous presence of nonlinear and boundary effects. It is worth observing that Eqs. (8), from which we derived our Eqs. (9), have been proposed by Cercignani [21] as boundary conditions in the linear regime. Thus, it would be interesting to explore whether in nonlinear situations they still lead to results which comply with the experimental data, or a generalization is necessary.

## Acknowledgments

D. Jou and F. X. Àlvarez acknowledge the financial support from the *Dirección General de Investigación* of the Spanish Ministry of Education and Science under grant FIS 2009-13370-C02-01, the *Consolider Project NanoTherm* (grant CSD-2010-00044), and the *Dirección General de Recerca* of the Generalitat of Catalunia under grant 2009-SGR-164.

A. Sellitto acknowledges the University of Basilicata for funding the research project *Modeling heat and electric transport in nanosystems in the presence of memory, nonlocal and nonlinear effects*, the financial support from the *Dirección General de Investigación* of the Spanish Ministry of Science and Innovation under grant FIS 2009-13370-C02-01 for his stay at the the Autonomous University of Barcelona, and the Italian *Gruppo Nazionale per la Fisica Matematica - GNFM*, for financial support under grant *Progetto Giovani 2012*.

V. A. Cimmelli acknowledges the financial support from the Italian *Gruppo Nazionale per la Fisica Matematica - GNFM*. Thanks are given to the University of Basilicata for financial support and for funding the research topic in Mathematical Physics *Equazioni constitutive per la conduzione del calore nei nanosistemi*.

## References

[1] C. C. Ackerman and R. A. Guyer. Temperature pulses in dielectric solids. *Annals of Physics* **50**, 128 (1968).
[2] F. X. Àlvarez, D. Jou, and A. Sellitto. Phonon hydrodynamics and phonon-boundary scattering in nanosystems. *J. Appl. Phys.* **105**, 014317 (2009).
[3] F. X. Àlvarez, D. Jou, and A. Sellitto. Pore-size dependence of the thermal conductivity of porous silicon: a phonon hydrodynamic approach. *Appl. Phys. Lett.* **97**, 033103 (2010).
[4] F. X. Àlvarez, D. Jou, and A. Sellitto. Phonon boundary effects and thermal conductivity of rough concentric nanowires. *J. Heat Transfer* **133**, 022402 (2011).
[5] V. M. Aroutiounian and M. Zh. Ghulinyan. Electrical conductivity mechanisms in porous silicon. *Phys. Status Solidi A* **197**, 462 (2003).
[6] M. Asheghi, Y. K. Leung, S. S. Wong, and K. E. Goodson. Phonon-boundary scattering in thin silicon layers. *Appl. Phys. Lett.* **71**, 1798 (1997).
[7] C. L. Bailey, R. W. Barber, D. R. Emerson, D. A. Lockerby, and J. M. Reese. A critical review of the drag force on a sphere in the transition flow regime. *AIP Conf. Proc.* **762**, 743 (2005).
[8] J. R. Baird, D. F. Fletcher, and B. S. Haynes. Local condensation heat transfer rates in fine passages. *Int. J. Heat Mass Transfer* **46**, 4453 (2003).
[9] A. Balandin and K. L. Wang. Effect of phonon confinement on the thermoelectric figure of merit of quantum wells. *J. Appl. Phys.* **84**, 6149 (1998).
[10] L. E. Bell. Cooling, heating, generating power, and recovering waste heat with thermoelectric systems. *Science* **5895**, 1457 (2008).
[11] G. Benedetto, L. Boarino, and R. Spagnolo. Evaluation of thermal conductivity of porous silicon layers by a photoacoustic method. *Appl. Phys. A: Mater. Sci. Process.* **64**, 155 (1997).
[12] G. Bergmann. Conductance of a perfect thin film with diffuse surface scattering. *Phys. Rev. Lett.* **94**, 106801 (2005).
[13] A. I. Boukai, Y. Bunimovich, J. Tahir-Kheli, J.-K. Yu, W. A. Goddard-III, and J. R. Heath. Silicon nanowires as efficient thermoelectric materials. *Nature* **451**, 168 (2008).
[14] H. C. Brinkman. A calculation of the viscous force exerted by a flowing fluid on a dense swarm of particles. *Appl. Sci. Res.* **A1**, 27 (1947).
[15] H. Bruus. *Theoretical microfluidics*. Oxford University Press, Oxford (2007).
[16] A. Burgdorfer. The influence of the molecular mean path on the performance of hydrodynamic gas lubricated bearings. *J. Basic Eng. - T. ASME* **8**, 94 (1959).
[17] L. T. Canham. Silicon quantum wire fabrication by electrochemical and chemical dissolution of wafers. *Appl. Phys. Lett.* **57**, 1046 (1990).
[18] B.-Y. Cao and Z.-Y. Guo. Equation of motion of a phonon gas and non-Fourier heat conduction. *J. Appl. Phys.* **102**, 053503 (2007).
[19] C. Cattaneo. Sulla conduzione del calore. *Atti Sem. Mat. Fis. Univ. Modena* **3**, 83 (1948).
[20] C. Cattaneo. A form of heat conduction equation which eliminates the paradox of instantaneous propagation. *Comput. Rend.* **247**, 431 (1958).
[21] C. Cercignani. *Higher order slip according to the linearized Boltzmann equation*. California Univ. Berkeley Inst. of Engineering Research, Report AS-64-19, Berkeley (1964).
[22] C. Cercignani. *Slow Rarefied Flows - Theory and Application to Micro-Electro-Mechanical Systems*. Birkhäuser Verlag, Basel (2006).

[23] G. Chen. *Nanoscale Energy Transport and Conversion - A Parallel Treatment of Electrons, Molecules, Phonons, and Photons*. Oxford University Press, Oxford (2005).
[24] J. D. Chung, , and M. Kaviany. Effects of phonon pore scattering and pore randomness on effective conductivity of porous silicon. *Int. J. Heat Mass Transfer* **43**, 521 (2000).
[25] V. A. Cimmelli. Different thermodynamic theories and different heat conduction laws. *J. Non-Equilib. Thermodyn.* **34**, 299 (2009).
[26] V. A. Cimmelli and K. Frischmuth. Nonlinear effects in thermal wave propagation near zero absolute temperature. *Physica B* **355**, 147 (2005).
[27] V. A. Cimmelli and K. Frischmuth. Gradient generalization to the extended thermodynamic approach and diffusive-hyperbolic heat conduction. *Physica B* **400**, 257 (2007).
[28] V. A. Cimmelli, A. Sellitto, and D. Jou. Nonlocal effects and second sound in a nonequilibrium steady state. *Phys. Rev. B* **79**, 014303 (2009).
[29] V. A. Cimmelli, A. Sellitto, and D. Jou. Nonequilibrium temperatures, heat waves, and nonlinear heat transport equations. *Phys. Rev. B* **81**, 054301 (2010).
[30] V. A. Cimmelli, A. Sellitto, and D. Jou. Nonlinear evolution and stability of the heat flow in nanosystems: Beyond linear phonon hydrodynamics. *Phys. Rev. B* **82**, 184302 (2010).
[31] J. E. Cornett and O. Rabin. Thermoelectric figure of merit calculations for semiconducting nanowires. *Appl. Phys. Lett.* **98**, 182184 (2011).
[32] E. Cunningham. On the velocity of steady fall of spherical particles through fluid medium. *Proc. R. Soc. Lond. A* **83**, 357 (1910).
[33] V. Dobrosavljević and G. Kotliar. Mean field theory of the Mott-Anderson transition. *Phys. Rev. Lett.* **78**, 3943 (1997).
[34] Y. Dong, B.-Y. Cao, and Z.-Y. Guo. Generalized heat conduction laws based on thermomass theory and phonon hydrodynamics. *J. Appl. Phys.* **110**, 063504 (2011).
[35] S. Volz (ed). *Thermal Nanosystems and Nanomaterials*. Springer, Berlin (2010).
[36] M. S. El-Genk and H. H. Saber. High efficiency segmented thermoelectric unicouple for operation between 973 and 300 K. *Energy Conversion and Management* **44**, 1069 (2003).
[37] J. Fang and L. Pilon. Scaling laws for thermal conductivity of crystalline nanoporous silicon based on molecular dynamics simulations. *J. Appl. Phys.* **110**, 064305 (2011).
[38] J. Fang and L. Pilon. Tuning thermal conductivity of nanoporous crystalline silicon by surface passivation: A molecular dynamics study. *Appl. Phys. Lett.* **101**, 011909 (2012).
[39] J. Fang, C. B. Kang, Y. Huang, S. H. Tolbert, and L. Pilon. Thermal conductivity of ordered mesoporous nanocrystalline silicon thin films made from magnesium reduction of polymer-templated silica. *J. Phys. Chem. C*, **116**, 12926 (2012).
[40] D. K. Ferry and S. M. Goodnick. *Transport in Nanostructures*. Cambridge University Press, Cambridge, England, second edition (2009).
[41] Y.-C. Fung. *Biomechanics: circulation*. Springer-Verlag, New York, second edition (1997).
[42] A. M. García-García. Classical intermittency and quantum Anderson transition. *Phys. Rev. E* **69**, 066216 (2004).
[43] G. Gesele, J. Linsmeier, V. Drach, J. Fricke, and R. Arens-Fischer. Temperature-dependent thermal conductivity of porous silicon. *J. Phys. D: Appl. Phys.* **20**, 2911 (1997).
[44] T. I. Gombosi. *Gaskinetic Theory*. Cambridge University Press, Cambridge (1994).
[45] I. Graur and F. Sharipov. Gas flow through an elliptical tube over the whole range of gas rarefaction. *Eur. J. Mech. B/Fluids* **27**, 335 (2008).
[46] Z.-Y. Guo. Motion and Transfer of Thermal Mass - Thermal Mass and Thermon Gas. *J. Eng. Term* **27**, 631 (2006).
[47] Z.-Y. Guo and Q.-W. Hou. Thermal wave based on the thermomass model. *J. Heat Trans - T. ASME* **132**, 072403 (2010).
[48] Z.-Y. Guo, B.-Y. Cao, H.-Y. Zhu, and Q.-G. Zhang. State equation of phonon gas and conservation equations for phonon gas motion. *Acta Phys. Sin.* **56**, 3306 (2007).
[49] R. A. Guyer and J. A. Krumhansl. Solution of the linearized phonon Boltzmann equation. *Phys. Rev.* **148**, 766 (1966).
[50] R. A. Guyer and J. A. Krumhansl. Thermal conductivity, second sound and phonon hydrodynamic phenomena in nonmetallic crystals. *Phys. Rev.* **148**, 778 (1966).

[51] N. G. Hadjiconstantinou. Comment on Cercignani's second-order slip coefficient. *Phys. Fluids* **15**, 2352 (2003).
[52] L. D. Hicks and M. S. Dresselhaus. Effect of quantum-well structures on the thermoelectric figure of merit. *Phys. Rev. B* **47**, 12727 (1993).
[53] L. D. Hicks and M. S. Dresselhaus. Thermoelectric figure of merit of a one-dimensional conductor. *Phys. Rev. B* **47**, 16631 (1993).
[54] R. J. Hill, D. L. Koch, and A. J. C. Ladd. Moderate-Reynolds-number flows in ordered and random arrays of spheres. *J. Fluid Mech.* **448**, 243 (2001).
[55] A. I. Hochbaum, R. Chen, R. D. Delgado, W. Liang, E. C. Garnett, M. Najarian, A. Majumdar, and P. Yang. Enhanced thermoelectric performance of rough silicon nanowires. *Nature* **451**, 163 (2008).
[56] P. E. Hopkins, P. M. Norris, L. M. Phinney, S. A. Policastro, and R. G. Kelly. Thermal Conductivity in Nanoporous Gold Films during Electron-Phonon Nonequilibrium. *Journal of Nanomaterials* **2008**, 418050 (2008).
[57] Y. T. Hsia and G. A. Domoto. An experimental investigation of molecular rarefaction effects in gas lubricated bearings at ultra-low clearance. *J. Lubr. Technol - T. ASME* **105**, 120 (1983).
[58] M.-J. Huanga, R.-H. Yena, and A.-B. Wang. The influence of the Thomson effect on the performance of a thermoelectric cooler. *Int. J. Heat Mass Transfer* **48**, 413 (2005).
[59] K. Imai. A new dielectric isolation method using porous silicon. *Solid-State Electronics* **24**, 159 (1981).
[60] G. Joshi, H. Lee, Y. Lan, X. Wang, G. Zhu, D. Wang, R. W. Gould, D. C. Cuff, M. Y. Tang, M. S. Dresselhaus, G. Chen, and Z. Ren. Enhanced Thermoelectric Figure-of-Merit in Nanostructured p-type Silicon Germanium Bulk Alloys. *Nano Lett.* **8**, 4670 (2008).
[61] D. Jou and L. Restuccia. Mesoscopic transport equations and contemporary thermodynamics: an introduction. *Contemp. Phys.* **52**, 465 (2011).
[62] D. Jou, J. Casas-Vázquez, and G. Lebon. Extended irreversible thermodynamics revisited (1988-1998). *Rep. Prog. Phys.* **62**, 1035 (1999).
[63] D. Jou, J. Casas-Vázquez, and G. Lebon. *Extended Irreversible Thermodynamics*. Springer, Berlin, fourth revised edition (2010).
[64] D. Jou, M. Criado-Sancho, and J. Casas-Vázquez. Heat fluctuations and phonon hydrodynamics in nanowires. *J. Appl. Phys.* **107**, 084302 (2010).
[65] D. Jou, G. Lebon, and M. Criado-Sancho. Variational principles for thermal transport in nanosystems with heat slip flow. *Phys. Rev. E* **82**, 031128 (2010).
[66] D. Jou, A. Sellitto, and F. X. Àlvarez. Heat waves and phonon-wall collisions in nanowires. *Proc. R. Soc. A* **467**, 2520 (2011).
[67] D. Jou, V. A. Cimmelli, and A. Sellitto. Nonlocal heat transport with phonons and electrons: Application to metallic nanowires. *Int. J. Heat Mass Transfer* **55**, 2338 (2012).
[68] E. H. Kennard. *Kinetic Theory of Gases*. McGraw-Hill, New York (1938).
[69] J. Y. Kim and B. J. Yoon. The effective conductivities of composites with cubic arrays of spheroids and cubes. *J. of Composite Materials* **33**, 1344 (1999).
[70] V. I. Kushch. Conductivity of a periodic particle composite with transversely isotropic phases. *Proc. R. Soc. A* **453**, 65 (1997).
[71] G. Lebon, D. Jou, J. Casas-Vázquez, and W. Muschik. Weakly nonlocal and nonlinear heat transport in rigid solids. *J. Non-Equilib. Thermodyn.* **23**, 176 (1998).
[72] G. Lebon, D. Jou, and J. Casas-Vázquez. *Understanding nonequilibrium thermodynamics*. Springer, Berlin (2008).
[73] G. Lebon, H. Machrafi, M. Grmela, and Ch. Dubois. An extended thermodynamic model of transient heat conduction at sub-continuum scales. *Proc. R. Soc. A* **467**, 3241 (2011).
[74] G. Lebon, D. Jou, and P. C. Dauby. Beyond the Fourier heat conduction law and the thermal non-slip condition. *Phys. Lett. A* **376**, 2842 (2012).
[75] H. Lee, D. Vashaee, D. Z. Wang, M. S. Dresselhaus, Z. F. Ren, and G. Chen. Effects of nanoscale porosity on thermoelectric properties of SiGe. *J. Appl. Phys.* **107**, 094308 (2010).
[76] J.-H. Lee, J. C. Grossman, J. Reed, and G. Galli. Lattice thermal conductivity of nanoporous Si: Molecular dynamics study. *Appl. Phys. Lett.* **91**, 223110 (2007).
[77] D. Li, Y. Wu, P. Kim, L. Shi, P. Yang, and A. Majumdar. Thermal conductivity of individual silicon nanowires. *Appl. Phys. Lett.* **83**, 2934 (2003).
[78] R. L. Liboff. *Kinetic theory (classical, quantum and relativistic description)*. Prentice Hall, Englewood Cliffs, New

Jersey (1990).
[79] W. Liu and M. Asheghi. Phonon-boundary scattering in ultrathin single-crystal silicon layers. *Appl. Phys. Lett.* **84**, 3819 (2004).
[80] H. Looyenga. Dielectric constants of heterogeneous mixtures. *Physica* **31**, 401 (1965).
[81] R. Luzzi, Á. R. Vasconcellos, and J. Galv ao Ramos. *Predictive Statistical Mechanics: A Nonequilibrium Ensemble Formalism (Fundamental Theories of Physics)*. Kluwer Academic Publishers, Dordrecht (2002).
[82] F. Márkus and K. Gambár. Heat propagation dynamics in thin silicon layers. *Int. J. Heat Mass Transfer* **56**, 495 (2013).
[83] P. Martin, Z. Aksamija, E. Pop, and U. Ravaioli. Impact of phonon-surface roughness scattering on thermal conductivity of thin Si nanowires. *Phys. Rev. Lett.* **102**, 125503 (2009).
[84] D. Mattia and F. Calabrò. Explaining high flow rate of water in carbon nanotubes via solid-liquid molecular interactions. *Microfluid Nanofluid* **13**, 125 (2012).
[85] R. A. Millikan. The general law of fall of a small spherical body through a gas, and its bearing upon the nature of molecular reflection from surfaces. *Phys. Rev.* **22**, 1 (1923).
[86] N. Mingo. Thermoelectric figure of merit and maximum power factor in III-V semiconductor nanowires. *Appl. Phys. Lett.* **84**, 2652 (2004).
[87] N. Mingo. Thermoelectric figure of merit of II-VI semiconductor nanowires. *Appl. Phys. Lett.* **85**, 5986 (2004).
[88] G. Mistura. Microfluidica, quando contaminarsi fa bene alla fisica. http://www.pd.infn.it/M5P/abstracts/mistura.htm (accessed 4 December 2012).
[89] Y. Mitsuya. Modified Reynolds equation for ultra-thin film gas lubrication using 1.5-order slip-flow model and considering surface accommodation coefficient. *J. Tribol - T. ASME* **115**, 289 (1993).
[90] D. Nakamura, M. Murata, H. Yamamoto, Y. Hasegawa, and T. Komine. Thermoelectric properties for single crystal bismuth nanowires using a mean free path limitation model. *J. Appl. Phys.* **110**, 053702 (2011).
[91] A. Pattamatta and C. K. Madnia. Modeling heat transfer in $Bi_2Te_3$-$Sb_2Te_3$ nanostructures. *Int. J. Heat Mass Transfer* **52**, 860 (2009).
[92] B. Poudel, Q. Hao, Y. Ma, Y. Lan, A. Minnich, B. Yu, X. Yan, D. Wang, A. Muto, D. Vashaee, X. Chen, J. Liu, M. S. Dresselhaus, G. Chen, and Z. Ren. High-Thermoelectric Performance of Nanostructured Bismuth Antimony Telluride Bulk Alloys. *Science* **320**, 634 (2008).
[93] B. Qui, L. Sun, and X. Ruan. Lattice thermal conductivity reduction in $Bi_2Te_3$ quantum wires with smooth and rough surfaces: A molecular dynamics study. *Phys. Rev. B* **83**, 035312 (2011).
[94] N. A. Roberts, D.G. Walker, and D. Y. Li. Molecular dynamics simulation of thermal conductivity of nanocrystalline composite films. *Int. J. Heat Mass Transfer* **52**, 2002 (2009).
[95] H. W. Russell. Principles of heat flow in porous insulators. *J. Am. Ceram. Soc.* **18**, 1 (1935).
[96] A. S. Sangani and A. Acrivos. Slow flow through a periodic array of spheres. *Int. J. Multiphase Flow* **8**, 343 (1982).
[97] A. S. Sangani and A. Acrivos. The effective conductivity of a periodic array of spheres. *Proc. R. Soc. A* **386**, 263 (1983).
[98] A. S. Sangani and A. Acrivos. Creeping flow through cubic arrays of spherical bubbles. *Int. J. Multiphase Flow* **9**, 181 (1983).
[99] C. B. Satterthwaite and R. W. Jr Ure. Electrical and thermal properties of $Bi_2Te_3$. *Phys. Rev.* **108**, 1164 (1957).
[100] A. Sellitto and V. A. Cimmelli. A continuum approach to thermomass theory. *J. Heat Trans. T. - ASME* **134**, 112402 (2012).
[101] A. Sellitto, F. X. Àlvarez, and D. Jou. Second law of thermodynamics and phonon-boundary conditions in nanowires. *J. Appl. Phys.* **107**, 064302 (2010).
[102] A. Sellitto, F. X. Àlvarez, and D. Jou. Temperature dependence of boundary conditions in phonon hydrodynamics of smooth and rough nanowires. *J. Appl. Phys.* **107**, 114312 (2010).
[103] A. Sellitto, F. X. Àlvarez, and D. Jou. Phonon-wall interactions and frequency-dependent thermal conductivity in nanowires. *J. Appl. Phys.* **109**, 064317 (2011).
[104] A. Sellitto, F. X. Àlvarez, and D. Jou. Geometrical dependence of thermal conductivity in elliptical and rectangular nanowires. *Int. J. Heat Mass Transfer* **55**, 3114 (2012).
[105] A. Sellitto, V. A. Cimmelli, and D. Jou. Analysis of three nonlinear effects in a continuum approach to heat transport in nanosystems. *Physica D* **241**, 1344 (2012).
[106] A. Sellitto, D. Jou, and J. Bafaluy. Nonlocal effects in radial heat transport in silicon thin layers and graphene

sheets. *Proc. R. Soc. A* **468**, 1217 (2012).
[107] A. Sellitto, D. Jou, and V. A. Cimmelli. A phenomenological study of pore-size dependent thermal conductivity of porous silicon. *Acta Appl. Math.* **122**, 435 (2012).
[108] A. Sellitto, V. A. Cimmelli, and D. Jou. Thermoelectric effects and size dependency of the figure-of-merit in cylindrical nanowires. *Int. J. Heat Mass Transfer* **57**, 109 (2013).
[109] G. J. Snyder and T. S. Ursell. Thermoelectric efficiency and compatibility. *Phys. Rev. Lett.* **91**, 148301 (2003).
[110] D. Song and G. Chen. Thermal conductivity of periodic microporous silicon films. *Appl. Phys. Lett.* **84**, 687 (2004).
[111] N. Stojanovic, D. H. S. Maithripala, J. M. Berg, and M. Holtz. Thermal conductivity in metallic nanostructures at high temperature: electrons, phonons, and the Wiedemann-Franz law. *Phys. Rev. B* **82**, 075418 (2010).
[112] B. Straughan. *Heat waves*. Springer, Berlin (2011).
[113] H. Struchtrup. *Macroscopic transport equations for rarefied gas flows: approximation methods in kinetic theory - Interaction of Mechanics and Mathematics*. Springer, New York (2005).
[114] J. Sturm, P. Grosse, and W. Theiss. Effective dielectric functions of alkali halide composites and their spectral representation. *Z. Phys. B: Condens. Matter* **83**, 361 (1991).
[115] P. J. Taylor, M. P. Walsh, and B. E. La Forge. Quantum dot superlattice thermoelectric materials and devices. *Science* **297**, 2229 (2002).
[116] Z. Tešanović, M. V. Jarić, and S. Maekawa. Quantum transport and surface scattering. *Phys. Rev. Lett.* **57**, 2760 (1986).
[117] D. Y. Tzou. *Macro to micro-scale heat transfer. The lagging behaviour*. Taylor and Francis, New York (1997).
[118] D. Y. Tzou. Nonlocal behavior in phonon transport. *Int. J. Heat Mass Transfer* **54**, 475 (2011).
[119] D. Y. Tzou and Z.-Y. Guo. Nonlocal behavior in thermal lagging. *Int. J. Thermal Sci.* **49**, 1133 (2010).
[120] A. Uhlir. Electrolytic shaping of germanium and silicon. *Bell Syst. Techn. J.* **35**, 333 (1956).
[121] F. T. Vasko and O. E. Raichev. *Quantum Kinetic Theory And Applications: Electrons, Photons, Phonons*. Springer, New York (2005).
[122] Y. Wanatabe, Y. Arita, T. Yokoyama, and Y. Igarashi. Formation and properties of porous silicon and its applications. *J. Electrochem. Soc: Solid-State Science and Technology* **122**, 1351 (1975).
[123] M. Wang, B.-Y. Cao, and Z.-Y Guo. General heat conduction equations based on the thermomass theory. *Frontiers Heat Mass Transfer* **1**, 013004 (2010).
[124] M. Wang, N. Yang, and Z.-Y. Guo. Non-Fourier heat conductions in nanomaterials. *J. Appl. Phys.* **110**, 064310 (2011).
[125] L. Wu. A slip model for rarefied gas flows at arbitrary knudsen number. *Appl. Phys. Lett.* **93**, 253103 (2008).
[126] Z. M. Zhang. *Nano/Microscale heat transfer*. McGraw-Hill, New York (2007).
[127] V. M. Zhdanov and V. I. Roldughin. Non-equilibrium thermodynamics and kinetic theory of rarefied gases. *Phys. Usp.* **41**, 349 (1998).
[128] J. M. Zide, D. O. Klenov, S. Stemmer, A. C. Gossard, G. Zeng, J. E. Bowers, D. Vashaee, and A. Shakouri. Thermoelectric power factor in semiconductors with buried epitaxial semimetallic nanoparticles. *Appl. Phys. Lett.* **87**, 112102 (2005).
[129] J. M. Ziman. *Electrons and Phonons*. Oxford University Press, Oxford (2001).